

Response to Report#1:

The authors have satisfactorily answered to the reviewers comments and it can be published in ACP after considering the following points.

1. *In the abstract please delete replace 'the humidification system (consists of two nephelometers ...in between)' by 'a humidified nephelometer system'. This is shorter and sounds better.*

Thanks for reviewer's suggestions. We have replaced 'the humidification system (consists of two nephelometers ...in between)' by 'a humidified nephelometer system' accordingly (Line 22 in the marked-up manuscript).

2. *Line 34: Add 'that' before 'NO3', Line 36: Add 'the' before 'humidograms'*

We have added 'that' before 'NO3' in Line 35 and 'the' before 'humidograms' in Line 37 in the marked-up manuscript.

3. *Concerning comment 10: The authors can use the values given in Tab. 1 in Zieger et al., 2014 and calculate backwards to retrieve the gamma or g-value (taking $c=0.9$).*

Taking $c=0.9$ and $f(85\%, 550\text{nm})=2.77$ (given in Tab. 1 in Zieger et al., 2014), we have retrieved the gamma value which equals to 0.59, which has been added to Table 5.

- I think a second proof reading of the manuscript by a native speaker is needed.

We have had a second proof reading by our native co-author.

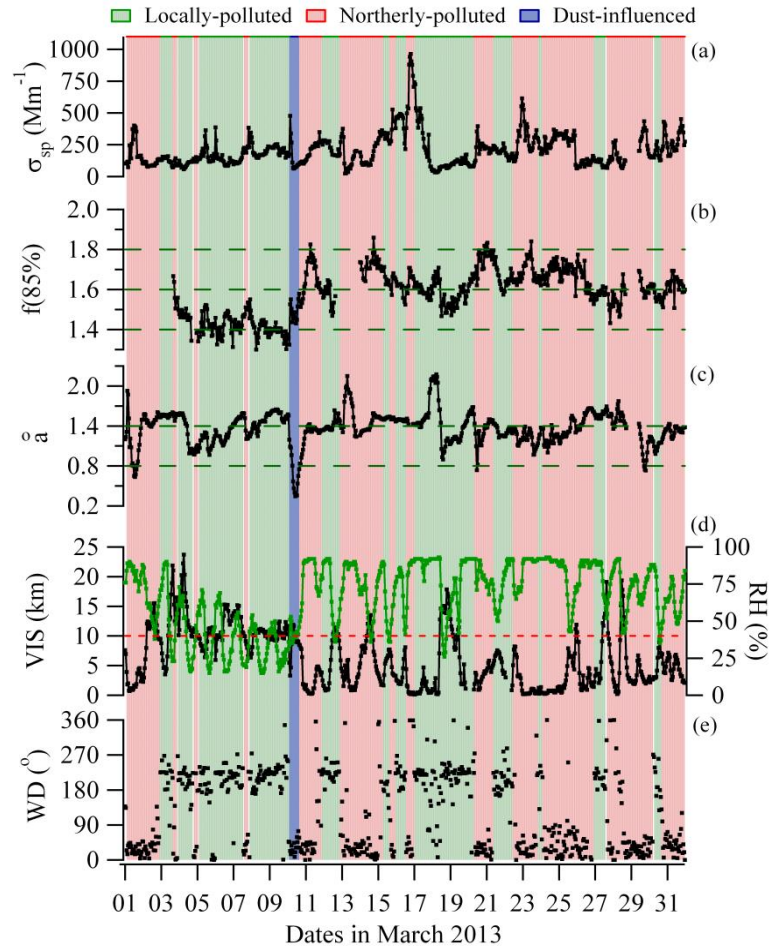
Response to Report#2:

1. *According to the question (comment 5) about the impact of the drying process on the results I would suggest to add your answer (in the reply letter) to the discussion of your results in the manuscript. This is essential information.*

Thanks for reviewer's suggestions. We have added this part to Sect. 2.4 Quality Control in Line 254-261 in the revised marked-up manuscript.

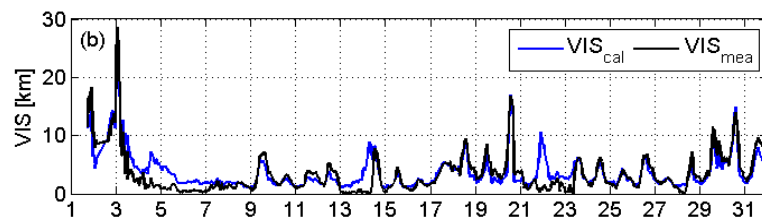
2. *Comment 9: Fig. 3. I am not satisfied with the presentation of these important results. You may color the segments or dots with respect to your air mass separation (red, green, blue). I would suggest to add some grid lines. Furthermore, you should re-arrange the graphs: (c)-(a)-(d)-(b)-[(e)] from measurement to meteorological data.*

We have changed the figure as the referee recommended. We have colored the segments according to the classification of the observation period and re-arranged the graphs.



3. Obviously you do not use the ambient relative humidity You (can) calculate the scattering coefficient with your parametrization for the ambient humidity for the entire measurement period and compare these results to the time line of the ambient visibility.

This is a very good suggestion, using our parameterization to calculate the scattering coefficients and visibility at ambient conditions and comparing the results with the measured visibility. We have done this comparison and the results shown below can be found in Shen et al. (2015, AE, underreview). The calculated visibility showed a quite similar pattern with the measured visibility except when the measured visibility was lower than 1 km and the corresponding RH was higher than 95%, the calculated visibility was always higher than the measured visibility.



Line:

21: ...scattering coefficients in the range of 40 to ~90% relative RH were measured...

We have revised this sentence in Line 22 in the revised marked-up manuscript according to the reviewer's suggestion.

31: Make two sentences: ...The highest values...

We have separated this sentence to two in Line 33 in the revised marked-up manuscript.

35-37: check the tense

We have checked the tense of that sentence and left it unchanged, but added "that" to explicitly set off the clause. The revised clause is "which suggests that NO_3^- played a vital role in aerosol hygroscopic growth during this study."

38: ...forcing is increased...

We have revised the sentence as

"Aerosol hygroscopic growth caused a 47% increase in the calculated aerosol direct radiative forcing at 85% RH, compared to the forcing at 40% RH" (Line 40-41 in the revised marked-up manuscript).

58: rephrase: "so as to have" (that they may have)

We have revised this sentence as

"to provide consistency within and among networks" (see Line 55 in the revised marked-up manuscript).

190: I would suggest to normalize your parameterization to 0% RH

Generally, aerosols at <40% RH can be considered as dry and the scattering coefficients would not change much below 40%. Many previous researchers have taken 40% as a reference for dry aerosol (Koloutsou-Vakakis et al., 2001; Carrico et al., 2003; Pan et al., 2009; Fierz-Schmidhauser et al., 2010). In this paper, we also regarded 40% as the value differentiating dry and wet. In addition, it is really hard to get RH=0 for ambient measurement.

232: remove "(as shown in Fig.2)"

We have removed "(as shown in Fig.2)" in Line 234 in the revised marked-up manuscript.

237/238: add "the" before Neph

This is a valid, general statement that applies to all humidograph systems other than only our humidograph system, so we prefer not adding "the" before Neph.

265/266: Grammar: The hourly averaged ...variedunder dry conditions, and the maximum...

We have revised this sentence (see Line 278-280 in the revised marked-up

manuscript).

269: I would prefer to mention the ambient and dry conditions within the text (as in the Fig.3 caption)

We have added the ambient conditions in the text (see Line 283 in the revised marked-up manuscript).

269 Please do not split value and unit (the same line for “6.2 km”)

We have revised that according to the reviewer’s suggestion.

270 was in a cloud or was in the clouds

We have changed to “in the clouds” (see Line 285 in the revised marked-up manuscript).

Fig 5, capture: Histogram ...

Yes, we have changed “Histograms” to “Histogram” (see Line 915 in the revised marked-up manuscript).

References in this response:

- Koloutsou-Vakakis, S., Carrico, C., Kus, P., Rood, M., Li, Z., Shrestha, R., Ogren, J., Chow, J., and Watson, J.: Aerosol properties at a midlatitude Northern Hemisphere continental site, *Journal of Geophysical Research*, 106, 3019-3032, 2001.
- Carrico, C. M., Kus, P., Rood, M. J., Quinn, P. K., and Bates, T. S.: Mixtures of pollution, dust, sea salt, and volcanic aerosol during ACE-Asia: Radiative properties as a function of relative humidity, *J. Geophys. Res.*, 108, 8650, 10.1029/2003JD003405, 2003.
- Pan, X. L., Yan, P., Tang, J., Ma, J., Wang, Z., Gbaguidi, A., and Sun, Y.: Observational study of influence of aerosol hygroscopic growth on scattering coefficient over rural area near Beijing mega-city, *Atmos. Chem. Phys.*, 9, 7519-7530, 2009.
- Fierz-Schmidhauser, R., Zieger, P., Gysel, M., Kammermann, L., DeCarlo, P., Baltensperger, U., and Weingartner, E.: Measured and predicted aerosol light scattering enhancement factors at the high alpine site Jungfraujoch, *Atmospheric Chemistry and Physics*, 10, 2319-2333, 2010.

Observations of relative humidity effects on aerosol light scattering in the Yangtze River Delta of China

Zhang Lu^{1,2}, Sun Junying^{1,3}, Shen Xiaojing¹, Zhang Yangmei¹, Che Haochi¹,
Ma Qianli⁴, Zhang Yiwen¹, Zhang Xiaoye¹, John A. Ogren⁵

¹ Key Laboratory of Atmospheric Chemistry of CMA, Institute of Atmospheric Composition, Chinese Academy of Meteorological Sciences, Beijing 100081, China

² College of Earth Science, University of Chinese Academy of Sciences, Beijing 100049, China

³ State Key Laboratory of Cryospheric Sciences, Cold and Arid Region Environmental and Engineering Research Institute, Chinese Academy of Sciences, Lanzhou 730000, China

⁴ LinAn Regional Atmosphere Background Station, LinAn 311307, China

⁵ Earth System Research Laboratory, NOAA, Boulder, CO, USA

Correspondence to: J.Y. Sun (jysun@cams.cma.gov.cn)

Abstract

Scattering of solar radiation by aerosol particles is highly dependent on relative humidity (RH) as hygroscopic particles take up water with increasing RH. To achieve a better understanding of the effect of aerosol hygroscopic growth on light scattering properties and radiative forcing, the aerosol scattering coefficients at RH in the range of ~40% to ~90% were measured using the humidification-a humidified nephelometer system (consists of two nephelometers operating in series with a humidifier in between) in the Yangtze River Delta of China in March 2013. In addition, the aerosol size distribution and chemical composition were measured. During the observation period, the mean and standard deviation (SD) of enhancement factors at RH=85% for the scattering coefficient ($f(85\%)$), backscattering coefficient ($f_b(85\%)$) and hemispheric backscatter fraction ($f_{\beta}(85\%)$) were 1.58 ± 0.12 , 1.25 ± 0.07

and 0.79 ± 0.04 , respectively, i.e. aerosol scattering coefficient and backscattering coefficient increased by 58 and 25% as the RH increased from 40 to 85%. Meanwhile, the aerosol hemispheric backscatter fraction decreased by 21%. The relative amount of organic matter (OM) or inorganics in PM_{10} was found to be a main factor determining the magnitude of $f(RH)$. The highest values of $f(RH)$ corresponded to the aerosols with a small fraction of OM, and vice versa. The relative amount of NO_3^- in fine particles was strongly correlated ~~to~~ with $f(85\%)$, which suggests that NO_3^- played a vital role in aerosol hygroscopic growth during this study. The mass fraction of nitrate also had a close relation to the curvature of the humidograms; higher mass fractions of nitrate were associated with humidograms that had the least curvature; ~~namely, the higher the nitrate concentration is, the straighter the humidogram will be.~~ Aerosol hygroscopic growth caused a 47% increase in the calculated aerosol direct radiative forcing at 85% RH, compared to the forcing at 40% RH. ~~At 85% RH, the aerosol direct radiative forcing was increased by 47% compared to that in dry conditions due to the aerosol hygroscopic growth.~~

1 Introduction

Hygroscopic aerosols take up water as humidity increases (Engelhart et al., 2011; Pilinis et al., 1989; Hänel, 1976; Covert et al., 1972). Aerosol water matters since water can affect both the size and refractive indices of atmospheric aerosols, thereby influencing the mass concentration, size distribution, and corresponding optical properties (e.g., scattering coefficient, backscattering coefficient, single scattering albedo, and asymmetry parameter) (Cheng et al., 2008; Randles et al., 2004; Malm et al., 2003; Carrico et al., 2003). In particular, understanding the effect of relative humidity on aerosol light scattering is important to better estimate the radiative forcing and evaluate visibility impairment (Ackerman et al., 2004; Tang, 1996; Charlson et al., 1992; Covert et al., 1972). Besides, most of the ground-based aerosol measurements are conducted in dry conditions ~~so as to~~ that they may have to provide consistency within and among networks. These measurements can differ significantly from the ambient ones. Thus, the determination of enhancement factors

for various optical variables are of crucial importance for climate forcing calculations (Quinn et al., 1995; Pilinis et al., 1995) and the comparison between remote sensing and ground based measurements (Zhang et al., 2012; Wang and Martin, 2007; Zieger et al., 2012).

The Yangtze River Delta, one of the most populated and fastest growing regions in China, has experienced extraordinary economic growth during the last two decades. Amounting to 2.1% of the land area of China, this region contains ~11% of the country's population and produces ~20% of China's Gross Domestic Product (GDP) in 2013 (Wang et al., 2013). Concurrent with population increase and economic growth are the increasing energy consumption and ~~growing~~ number of automobiles, ~~and therefore, causing~~ the Yangtze River Delta ~~has to~~ become a significant source of gas and particulate pollutants and secondary aerosol production. A 5-week field campaign was carried out in the early winter of 1999 at LinAn, a background station in the Yangtze River Delta (Xu et al., 2002). However, since then the physical and chemical properties of gas and particulate pollutants have changed dramatically with the rapidly developing economy and fast growing population, e.g. from 1999 to 2013, the sulfate mass concentration decreased from 21.2 ± 1.5 to 8.1 ± 4.1 (mean \pm SD) (Qi et al., 2012; Xu et al., 2008; ZEPB, 1999; ZEPB, 2013). In order to better understand the aerosol light scattering properties and their dependency on relative humidity in the Yangtze River Delta, both the scattering and backscattering coefficients under dry (RH<40%) conditions and controlled, elevated relative humidity were measured, along with the chemical composition and particle number size distribution.

The enhancement factors discussed in this work include scattering enhancement factor $f(\text{RH}, \lambda)$, enhancement factor for backscattering coefficient $f_b(\text{RH}, \lambda)$ and enhancement factor for hemispheric backscatter fraction $f_\beta(\text{RH}, \lambda)$. The impact of relative humidity on the aerosol light scattering coefficient is called the ~~defined as~~ scattering enhancement factor $f(\text{RH}, \lambda)$, defined as

$$f(\text{RH}, \lambda) = \sigma_{\text{sp}}(\text{RH}, \lambda) / \sigma_{\text{sp}}(\text{dry}, \lambda) \quad (1)$$

where $\sigma_{\text{sp}}(\text{dry}, \lambda)$ and $\sigma_{\text{sp}}(\text{RH}, \lambda)$ represent scattering coefficients at wavelength λ in dry

conditions and at a defined higher relative humidity, respectively.

Likewise, the impact of relative humidity on aerosol backscattering coefficient can be described as [the](#) enhancement factor for backscattering coefficient $f_b(RH, \lambda)$:

$$f_b(RH, \lambda) = \sigma_{bsp}(RH, \lambda) / \sigma_{bsp}(dry, \lambda) \quad (2)$$

where $\sigma_{bsp}(dry, \lambda)$ and $\sigma_{bsp}(RH, \lambda)$ represent backscattering coefficients at wavelength λ in dry conditions and at a defined relative humidity, respectively. $f(RH, \lambda)$ and $f_b(RH, \lambda)$ are always greater than 1 if no significant restructuring is taken place after water uptake (Weingartner et al., 1995).

Hemispheric backscatter fraction ($b = \sigma_{bsp} / \sigma_{sp}$) is closely related to the upscatter fraction ($\bar{\beta}$), the fraction of incident solar radiation scattered into space (Wiscombe and Grams, 1976). The impact of relative humidity on aerosol hemispheric backscatter fraction can be defined as [the](#) enhancement factor for hemispheric backscatter fraction $f_{\beta}(RH, \lambda)$ ([Adam et al., 2012](#)):

$$f_{\beta}(RH, \lambda) = b(RH, \lambda) / b(dry, \lambda) \quad (3)$$

where $b(dry, \lambda)$ and $b(RH, \lambda)$ represent hemispheric backscatter fraction at wavelength λ in dry conditions and at the defined relative humidity. ~~b is defined as the ratio of backscattering coefficient to scattering coefficient: $b = \sigma_{bsp} / \sigma_{sp}$.~~ Thus, $f_{\beta}(RH, \lambda)$ can be rewritten as: $f_{\beta}(RH, \lambda) = f_b(RH, \lambda) / f(RH, \lambda)$.

The wavelength dependence of scattering enhancement factor $f(RH, \lambda)$ varies with generalized aerosol types. Kotchenruther and Hobbs (1998) and Zieger et al. (2010; 2011) found no pronounced wavelength dependence of $f(RH, \lambda)$ for biomass burning aerosols and arctic aerosols, respectively; Zieger et al. (2013) found small variations (<5%) of $f(RH, \lambda)$ at 450, 550 and 700 nm for several European sites; Kotchenruther et al. (1999) and Magi and Hobbs (2003) reported significant wavelength dependence of $f(RH, \lambda)$ for urban/industrial aerosols off the east coast of the United States. In this study, the wavelength dependence of enhancement factors was also investigated. Except when specially mentioned, all the parameters discussed in this study are based on the measurements at 550 nm wavelength only.

2 Experimental sites and instrumentation

2.1 Site description

This study was carried out during an intensive field sampling period from 1 to 31 March 2013 at LinAn Regional Atmosphere background station, which is a WMO GAW regional station (30.3 °N, 119.73 °E, 138 m a.s.l.) located in the center of [the](#) Yangtze River Delta, China (Fang et al., 2013) (as shown in Fig. 1). It is approximately 11 km north of the city of LinAn, with a population of 1.5 million. The site is ~50 km west of Hangzhou (capital of Zhejiang Province with a population of ~8.8 million) and ~210 km southwest of Shanghai (a mega-city with a population of ~20 million). LinAn station is on the top of a small hill, in an area primarily covered by bamboo forests and paddy rice fields, and represents the background conditions of the Yangtze River Delta. North of the station is a small village with ~200 inhabitants. In addition, there is an activated charcoal factory ~1.4 km north of LinAn station that uses bamboo wood as its source material (Qi et al., 2012). During the observation period, the prevailing winds were northeasterly (NE) and southwesterly (SW) with an average wind speed of $\sim 2.5 \text{ m s}^{-1}$ (SD 1.4 m s^{-1}). 72-hour back trajectories showed two contrasting air mass origins: (1) air masses from Northern China through long-distance transport and (2) air masses from southerly/southwesterly directions with a much shorter transport distance.

2.2 Measurement system and data processing

The scattering enhancement factor $f(\text{RH})$ is defined as the ratio of aerosol scattering coefficient at a given, elevated RH to that at a low RH (usually <40%). Correspondingly, the humidification system, [called a humidograph](#), included two nephelometers operating in series with a humidifier between them. Sample air entered the first nephelometer (reference nephelometer or DryNeph) through an aerosol dryer (Shen et al., 2011; Tuch et al., 2009) to ensure the aerosol was at dry conditions (RH inside DryNeph was $12.2 \pm 3.4\%$ (mean \pm SD) for the whole field campaign), then passed through the humidifier, where the sample RH was regulated to a higher RH that was ramped from ~40 to 90%, and finally entered the second nephelometer (humidified nephelometer or WetNeph) where the scattering coefficient of humidified

aerosols was measured.

Aerosol total scattering (between 7 and 170 degrees) and backscattering coefficients (between 90 and 170 degrees) were measured ~~by~~with an integrating nephelometer (TSI Inc., Model 3563) at three wavelengths: blue (450 nm), green (550 nm) and red (700 nm). Data were recorded as 1-minute averages and a zero check was performed automatically once per hour. The detailed ~~information~~characteristics of this instrument has been described in many previous studies (Anderson and Ogren, 1998; Charlson et al., 1969; Anderson et al., 1996).

The humidifier was built by the aerosol group in Global Monitoring Division, Earth System Research Laboratory, National Ocean & Atmospheric Administration, USA (NOAA/GMD), ~~which was based on the design~~ described in Carrico et al. (1998). It ~~consists~~consisted of 2 concentric tubes with a heater and insulation around the outer tube. Sample air ~~flows~~flowed through the inner tube, while water ~~circulates~~circulated between the inner and outer tubes. The inner tube ~~is~~was made of porous extruded PTFE (polytetrafluoroethylene) membrane, whose pore size is large enough for water molecules, but too small for larger molecules such as oxygen to cross. The flux of water vapor through the membrane ~~is~~was controlled by regulating the electric current to the humidifier heater until the desired RH ~~is~~was attained. The humidity scan was a one-hour cycle; RH was ramped from ~40 to 90% during the first half hour and in the reverse direction during the last half hour.

Besides the scattering measurement, particle number size distribution and aerosol chemistry were also measured at the station. Particle number size distributions from 3 nm to 10 μm were measured ~~by~~with a twin differential mobility particle sizer (TDMPS) (Birmili et al., 1999) and an aerodynamic particle sizer (APS, model 3321, TSI Inc.). The mass concentrations of sulfate, nitrate, ammonium, organic matter (OM) and chloride (aerodynamic diameter less than 1 μm) were measured ~~by~~with an aerosol mass spectrometer (AMS, Aerodyne Inc.). The equivalent mass concentration of black carbon (EBC) was measured ~~by~~with a multi angle absorption photometer (MAAP, model 5012, Thermo Scientific Inc.) at 637 nm wavelength (Müller et al., 2011); ~~the~~ the assumed mass absorption cross-section was $6.6 \text{ m}^2\text{g}^{-1}$. Visibility was

measured using a near-forward scattering sensor (FD12, Vaisala). Meteorological data were provided by the LinAn Regional Atmosphere Background Station.

All the instruments were housed in a measurement laboratory where room temperature was controlled at $\sim 25 \pm 1^\circ\text{C}$. All data were reported in Beijing Time (BJT=UTC+8 h) and all the scattering data were referenced at $T=0^\circ\text{C}$ and $P=1013.25$ hPa. The truncation error correction, proposed described by Anderson and Ogren in (1998) (Anderson and Ogren, 1998), was applied to retrieve the final scattering and backscattering coefficients. The Ångström exponent α was defined as $\alpha = -\log[\sigma_{\text{sp}}(\lambda_1)/\sigma_{\text{sp}}(\lambda_2)]/\log[\lambda_1/\lambda_2]$. It represented the wavelength dependence of light scattering assuming a power law relationship of σ_{sp} and σ_{bsp} with wavelength. In this study, scattering coefficients at 450 nm and 700 nm were used to derive α . Normalization of $f(\text{RH})$ (Day and Malm, 2001) has been carried out to get the final $f(\text{RH})$ scan values, i.e. $f(40\%)$ (the lowest RH in one cycle) is set to 1 and used to normalize other $f(\text{RH})$ values in this cycle. It's worth mentioning that the normalization of $f(\text{RH})$ (see Sect. 2.2) may underestimate $f(\text{RH})$ to some extent, since some organics (e.g. humic acid sodium) take up water even when $\text{RH} < 40\%$ (Sjogren et al., 2007; Dick et al., 2000). To evaluate its impact, we calculated the raw $f(40\%)$ value without the normalization. The average and standard deviation were 1.03 and 0.03 with a maximum of 1.08, which means this normalization may cause an underestimate of 5% (an error of 3% was caused by the inconsistency of DryNeph and WetNeph, see Sect. 2.4) at most. Figure 2c shows the un-normalized $f(\text{RH})$ value, the lowest value of each cycle was around 1.03, considering which represents the inconsistency of DryNeph and WetNeph, $f(\text{RH})$ is close to unity at the lowest RH ($\sim 40\%$).

2.3 Inlet system

An automatic regenerating adsorption aerosol dryer (Tuch et al., 2009) was used to provide low RH sample air to DryNeph, TDMPS, APS, AMS and MAAP to ensure comparability of measurements. The aerosol dryer was housed in a separate shelter which that was located on the rooftop (~ 5 m a.g.l.) of the measurement laboratory. Aerosols-Sample air entered the shelter through a commercially available PM_{10}

impactor (PM₁₀ inlet, URG Corporation). ~~Then these particles) and then went passed~~
through the adsorption aerosol dryer (Tuch et al., 2009) to ~~ensure-reduce~~ the RH ~~to~~
less than 30%. The dried ~~aerosols-sample~~ passed through a ~~3/4-inch diameter stainless~~
~~tube to a manifold, which split the sample into 1/4 or 3/8-inch diameter tubes that~~
~~connected to the splitter via 3/4" stainless steel tubes, and then reached~~ different
instruments. The total sample flow through ~~this dryer inlet~~ ~~the PM₁₀ impactor~~ was kept
at 16.7 lpm to ensure a 50% collection efficiency at 10 μm aerodynamic diameter
(Bernier et al., 1979). ~~Since a lot of instruments share the total flow, the sample flow~~
~~for the nephelometer is 9 lpm.~~

2.4 Quality control ~~on scattering measurements~~

Accurate performance of nephelometers and RH sensors is crucial to retrieve
reliable enhancement factors ($f(\text{RH}, \lambda)$, $f_b(\text{RH}, \lambda)$ and $f_\beta(\text{RH}, \lambda)$), since they are defined
as the ratio of aerosol scattering coefficient/ backscattering coefficient/ hemispheric
backscatter fraction at a higher RH to those at a low RH (usually <40%). In addition,
the RH control in the WetNeph sensing volume is also critical to $f(\text{RH})$ measurement.
Therefore, several comparisons and calibrations have been carried out before and
during the experiment. Three external RH sensors (Vaisala, model HMP60) were
calibrated in the RH range of 11% to 80% using a Vaisala Humidity Calibrator
(HMK15) with four saturated salt solutions (LiCl, K₂CO₃, NaCl, (NH₄)₂SO₄), and a
humidity/temperature transmitter (Vaisala, model HMT333), which was calibrated by
the National Center for Meteorological Metrology, China. The two internal
nephelometer RH sensors were calibrated to the external RH sensors with an
uncertainty of $\leq 2\%$. A good agreement of these RH sensors was achieved with ~~the a~~
~~discrepancy~~ of <3%. Both nephelometers were calibrated with CO₂ (purity 99.999%)
and filtered air. Filtered air measurements were made automatically every hour to
track the instrument stability background. Comparison of scattering and backscattering
coefficients of the two nephelometers under-at low RH ($9.6 \pm 3.2\%$) was performed
during 1 to 3 March, 2013 ~~(as shown in Fig. 2)~~. The total scattering coefficient and
backscattering coefficient measured by WetNeph were constantly 3% ($y=1.03x+1.60$,
 $R^2=1.000$) and 4% ($y=1.04x+0.09$, $R^2=0.997$) higher than those obtained by DryNeph

at 550 nm (similarly for other wavelengths); the high consistency demonstrates that the two nephelometers were operating quite steadily and the scattering/backscattering coefficients measured by DryNeph can be corrected in order to make them comparable to the measurements of WetNeph. The uncertainty of nephelometer measurements ~~was~~is ~10% (Anderson et al, 1996), ~~which, when combining combined with~~ the uncertainty of the measurements of the internal RH sensors, ~~yields~~ ~~the~~ uncertainty ~~of for~~ f(85%) ~~was of~~ ~20%. ~~This overall uncertainty could be lower at large, which may decrease~~ for less hygroscopic particles or ~~smaller lower~~ RHs.

The RH at the outlet of WetNeph was regulated via a feedback system ~~between using~~ the Vaisala RH signal, a PID controller and a heater. The humidifier set point was stepped from low to high RH and back to low RH every hour with the set point changing every one or two minutes. Figure 2 is an example of our data showing the ~~relative humidity RH~~ control and corresponding scattering measurements. As can be seen from Fig. 2, good ~~relative humidity RH~~ control was achieved ~~no matter whether regardless of the magnitude of~~ the scattering ~~backscattering~~ coefficient ~~was high or low~~.

~~During the drying and humidifying process, thermophoresis, coagulation, evaporation, and irreversible chemical reactions and so on can differentiate alter the particles from the original ones. A variety of measures were taken to minimize changes to the particles: In that case, we have made efforts to retain the aerosol property. The transport path was made as short and straight as possible, particle-free air was diluted to the aerosol stream to reduce coagulation, and lower RH and higher heater temperatures was were avoided to reduce evaporation of as it will result in semi-volatile compounds like weak organic acids and nitrates evaporating from aerosols.~~

The nephelometers were operated at a constant flow of 20 lpm, comprised of 9 lpm sample air and 11 lpm particle-free air (dilution flow). The total flowrate through the nephelometer was controlled by a mass flow controller. The dilution flow was regulated by a needle valve and measured ~~by with~~ a mass flowmeter. The sample and dilution flow have been calibrated with a Gilibrator bubble flowmeter before the

experiment. Filtered air tests ~~have were~~ also ~~been~~ conducted to make sure that all the instruments were in good condition and that there were no leaks in the system.

3 Results and discussion

3.1 Overview

Figure 3 shows the time series of the measured and derived aerosol variables ~~in~~ during March 2013, as well as the ambient RH and visibility. The scattering enhancement factor $f(85\%)$ ranged from 1.29 to 1.86 (~~as shown in~~ Fig. 3a) with an average of 1.58 (Table 1) for the whole campaign. During 4-9 March, when LinAn was dominated by air masses from the south under clear sky, $f(85\%)$ stayed at a low value of $1.42 (\pm 0.05)$ ~~when LinAn was dominated by air masses from the south under clear sky~~. In March, the hourly averaged aerosol scattering coefficient, measured under dry conditions ~~under dry conditions~~ (~~shown in~~ Fig. 3c), varied from 21 to 1067 Mm^{-1} under dry conditions, and the maximum occurred on 16 March, when a severe haze occurred. The mean value and standard deviation of the hourly averaged aerosol scattering coefficient was 223 Mm^{-1} (140 Mm^{-1}). Visibility (Fig. 3b) varied from 0.1 km to 23.7 km at ambient conditions with a mean value of 6.2 km. ~~It was quite low~~ The lowest visibilities were observed on 23 and 24 March, when ~~because~~ the station was in the clouds. From 15 to 16 March, visibility declined to 4.4 km with the accumulation of pollutants in the atmosphere, which was a severe haze episode (as mentioned above). An air mass from Northwest China with high dust levels arrived at LinAn on 10 March, with an abrupt increase of the aerosol scattering coefficient (Fig. 3c) and a sharp decline of Ångström exponent (Fig. 3d).

Based on nephelometer measurements, the enhancement factors for scattering coefficient $f(\text{RH})$, backscattering coefficient $f_b(\text{RH})$ and hemispheric backscatter fraction $f_\beta(\text{RH})$ were determined by using Eq. (1), (2) and (3), respectively. ~~As can be seen from Table 1,~~ Their values at different RHs (50, 60, 70, 80 and 85%) were obtained using linear interpolation from the half-hourly humidogram data (Table 1). The enhancement factors $f(\text{RH})$ and $f_b(\text{RH})$ increased as the RH increased, but $f_b(\text{RH})$ increased much more slowly than $f(\text{RH})$. The $f(85\%)$ and $f_b(85\%)$ were 1.58 and 1.25,

respectively, suggesting that the scattering coefficient and backscattering coefficient at 85% RH were 58 and 25% higher than those in dry conditions due to aerosol water uptake. The $f_{\beta}(\text{RH})$ decreased with increasing RH, i.e. hemispheric backscatter fraction becomes smaller with the increase of RH and the fraction of radiation that would be backscattered into space was reduced. The $f_{\beta}(\text{RH})$ decreased ~21% as the RH increased from 40 to 85%. All these parameters are of crucial importance in evaluating the aerosol radiative forcing.

Generally, the scattering enhancement factor ($f(80\%)=1.44$) is much lower than the result ($f(80\%)=1.7\text{--}2.1$) obtained by Xu et al. (2002) for LinAn in 1999. This value is also lower than the results obtained by Carrico during ACE-1 (Carrico et al., 1998) and ACE-Asia (Carrico et al., 2003), the values obtained by Zieger et al. (2013) in several European sites and the Arctic, as well as the values ~~achieved-reported at several sites in the U.S. by Malm and Day~~ (Malm et al., 2005; Malm et al., 2003; Malm and Day, 2001; Day and Malm, 2001; Malm and Day, 2000) ~~in America~~. However, the difference between measured $f(\text{RH})$ in this study and previous studies performed in China (Yan et al., 2009; Pan et al., 2009; Liu et al., 2009; ~~Delene and Ogren, 2002~~; Cheng et al., 2008) are much smaller. The enhancement factors for backscattering coefficient and hemispheric backscatter fraction ($f_b(85\%)$ and $f_{\beta}(85\%)$) ~~is—were~~ 1.25(0.07) and 0.79(0.04), respectively, similar to the results ($f_b(82\%)=1.22\pm0.06$ and $f_{\beta}(82\%)=0.83$) obtained by Carrico at Sagres, Portugal during ACE-2 (Carrico et al., 2000) and the results ($f_b(82\%)=1.27$ and $f_{\beta}(82\%)=0.75$) obtained by Carrico et al. (2003) during the dust-dominant period in ACE-Asia.

3.2 Aerosol chemical properties

The submicron mass concentrations of sulfate, nitrate, ammonium, chloride and organic matter (OM) measured by AMS, ~~and plus~~ EBC in PM_{10} measured by MAAP, are summarized in Table 2. The mass concentration of OM is the largest, while the mass concentration of chloride is the smallest, in accord with previous studies in LinAn (Meng et al., 2012; Yan et al., 2005). The mean mass concentrations of nitrate and sulfate were $9.8\pm12.1\text{ }\mu\text{g}\cdot\text{m}^{-3}$ and $8.1\pm4.1\text{ }\mu\text{g}\cdot\text{m}^{-3}$ in this study, similar to the values ($9.4\pm7.1\text{ }\mu\text{g}\cdot\text{m}^{-3}$ for nitrate and $8.6\pm3.7\text{ }\mu\text{g}\cdot\text{m}^{-3}$ for sulfate in $\text{PM}_{2.5}$) at LinAn in

~~summer~~, 2010 ~~summer~~ (Meng et al., 2012).

Aerosol acidity is a key parameter affecting aerosol hygroscopic growth. It is usually examined by comparing the NH_4^+ mass concentration ~~measured by AMS~~ and the amount needed to fully neutralize sulfate, nitrate and chloride ions ($\text{NH}_4^+_{\text{predicted}}$) (Sun et al., 2010):

$$\text{NH}_4^+_{\text{predicted}} = 18 \times (2 * \text{SO}_4^{2-}/96 + \text{NO}_3^-/62 + \text{Cl}^-/35.5) \quad (4)$$

Figure 4 illustrates the relationship of measured NH_4^+ and predicted NH_4^+ . As shown in Fig. 4, the regression slope is close to 1, which implies that there was sufficient NH_3 in the atmosphere to neutralize H_2SO_4 , HNO_3 and HCl , and that the PM_{10} aerosol at LinAn was bulk neutralized during the measurement period. Therefore, the dominant chemical form of sulfate aerosol is ammonium sulfate (AS) rather than acidic sulfate (H_2SO_4 or NH_4HSO_4) and the nitrate existed in the form of NH_4NO_3 (AN). By calculating Pearson's correlation coefficient among 5 different chemical ~~composition species~~, it ~~could be was~~ found that NH_4^+ and NO_3^- are strongly correlated with $r=0.93$; NH_4^+ and SO_4^{2-} , Cl^- are highly related with r equal to 0.77 and 0.74 respectively, which also implies the main form of inorganics would be NH_4NO_3 , $(\text{NH}_4)_2\text{SO}_4$ and NH_4Cl . However, ~~because~~ the average mass concentration of chloride was very low (see Table 2) at LinAn, ~~it suggests that and~~ NH_4NO_3 and $(\text{NH}_4)_2\text{SO}_4$ ~~are were~~ the dominant water-soluble ionic species, ~~which are~~ consistent with previous results at LinAn based on filter chemical measurements (Meng et al., 2012).

3.3 Wavelength dependence of the scattering enhancement factor $f(85\%)$

The wavelength dependence of ~~the~~ scattering enhancement factor is needed to estimate the aerosol radiative forcing since solar radiation at Earth's surface depends on wavelength. The histogram for $f(85\%, 550 \text{ nm})$ is shown in Fig. 5. Overlaid on the histogram for $f(85\%, 550 \text{ nm})$ (Fig. 5) are Gaussian curves based on the statistics for $f(85\%)$ at each wavelength. No apparent shift of mean $f(85\%)$ is seen for the 550 nm and 700 nm wavelength pair (see Fig. 5); while the mean $f(85\%, 450 \text{ nm})$ is ~6% lower than that at 550 nm with a smaller standard deviation (see Fig. 5). For higher

values (90th and 70th percentile values in Table 3), ~~slightly-a slight~~ wavelength dependence of $f(RH)$ can be observed, i.e. the $f(RH)$ increases with the increase of wavelength. However, the differences are mostly under 10% —and therefore the discussion is focused on 550 nm wavelength in this study. Similar results were obtained by Zieger at a regional continental research site at Melpitz, Germany (Zieger et al., 2014).

3.4 Classification of various observation episodes

Based on wind direction, back trajectory analysis and weather phenomena, the observation periods can be classified into three main sectors: a northerly-polluted period (influenced by long-distance transport from northern China), a locally-polluted period, and a dust-influenced episode. Air mass back trajectories over 72 hours at 300m a.g.l. arrival height were calculated using the Trajectory Statistics (TrajStat) model (Wang et al., 2009) with 6-hourly archived meteorological data provided by the US National Centers for Environmental Prediction (NCEP). The characteristics of these three periods are as follows:

1. Periods when the wind direction is between 120° and 270° are ~~chosen~~ labelled as “locally-polluted periods”. During ~~this-these~~ periods, pollutants mostly came from Anhui province, Jiangxi province and the southern region of Zhejiang province as well as LinAn (green line in Fig. 6). Economy in these areas is mainly made up of manufacturing, tourism and agriculture.
2. Periods when the wind direction ~~is-was~~ greater than 270° or less than 120° are described as “northerly-polluted periods”. Back trajectories indicate that most of the air masses came from northern China and passed over heavily polluted areas such as the Beijing-Tianjin-Tangshan economic region and the Yangtze River Delta during long-distance transport (red line in Fig. 6).
3. A heavy dust event occurred at LinAn on 10 March (approximately from 02:00 BJT) according to satellite information (<https://earthdata.nasa.gov/labs/worldview/>) and meteorology information (provided by China Meteorological Administration, CMA). The 72 h back trajectory shows the air masses tracked from Mongolia and passed over Inner Mongolia (blue line in Fig. 6).

3.4.1 Locally-polluted periods

~~In~~ During the periods of 4-9, 15-20 and 26-30 March, 2013, aerosols were mainly from local locally mixed pollutants pollution sources from in Zhejiang and/or nearby provinces. The mean $f(80\%)$ and $f(85\%)$ were 1.36 and 1.52 (as shown in Table 4), ~10 and 8% lower than those in northerly-polluted periods.

The enhancement factor for scattering ~~coefficient~~ and backscattering coefficients at 80% during locally-polluted periods ~~is was~~ 1.36 and 1.15, respectively, similar to the values ($f(82.5\%)=1.4-1.5$) and ($f_{\beta}(82.5\%)=1.1-1.2$) obtained by Koloutsou-Vakakis et al. (2001) at a ~~northern hemisphere,~~ continental U.S. site (Bondville, Illinois, US). The measured dry scattering coefficient ~~is was~~ 217 Mm^{-1} , ~15% lower than that of the northerly-polluted period (251 Mm^{-1}). The averaged mass percentages of sulfate, nitrate, ammonium, OM, chloride and EBC ~~are were~~ 17.6, 16.1, 13.0, 42.2, 1.5 and 9.6%, respectively (~~shown in~~ Fig. 6a); for this and subsequent calculations of mass percentages, the denominator is the sum of the mass concentrations of sulfate, nitrate, ammonium, OM, chloride and EBC. Compared to the northerly-polluted period, the mass percentage of OM ~~is was~~ ~27% higher during the locally-polluted period, while the mass percentage of nitrate ~~is was~~ ~33% lower. Although the $\text{OM}/(\text{OM}+\text{SO}_4^{2-})$ ratios during locally-polluted ~~period~~ (~0.70) and northerly-polluted periods (~0.67) ~~are were~~ similar, the $\text{OM}/(\text{OM}+\text{NO}_3^-+\text{SO}_4^{2-})$ ratio during the locally-polluted periods (~0.56) ~~is was~~ 24% higher than that during the northerly-polluted periods (~0.45), which may partly explain the lower $f(\text{RH})$ during locally-polluted episodes (as discussed later in Sect. 3.5).

3.4.2 Northerly-polluted periods

The air masses reaching LinAn during the periods March 1-3, 11-15, 20-26 and 30-31 (dust episode excluded) mainly came from northern China through long-distance transport. The mean $f(80\%)$ and $f(85\%)$ were 1.50 and 1.64, respectively (as shown in Table 4).

The value ($f(80\%)=1.50$) is similar to the previous results ($f(80\%)=1.48$) obtained by Yan et al. (2009) for periods ~~under the downwind of~~ influenced by the urban plume from Beijing, ($f(80\%)=1.46\pm0.10$) reported by Carrico et al. (2000) for

anthropogenic aerosols in Europe during the 2nd Aerosol Characterization Experiment (ACE-2) campaign, and $f(80\%)=1.55-1.59$ indicated by Pan et al. (2009) for a rural site (Xin'an) near Beijing city during pollution periods. However, the measured $f(80\%)$ was much lower than $f(80\%)=2.0-2.43$ during a pollution episode reported by Kim et al. (2006) at the Gosan regional background site, 720 km northeast of LinAn and results $f(82\%)=2.24\pm0.20$ obtained by Carrico et al. (2003) in ACE-Asia for polluted air masses measured over the ocean. The $f(RH)$ of continental air masses transported over the ocean was higher than that over the continent, and the possible mechanisms for that increase might include coagulation with sea-salt particles and the oxidation of SO_2 and VOCs (volatile organic compounds) leading to an increase in ~~the~~ particle's aerosol hygroscopicity.

3.4.3 Dust-influenced episode

During a severe cold air outbreak, a strong dust event struck northern China on 8 and 9 March, 2013. The affected area covered about 2.8 million square kilometers, about ~~0.27 million square kilometers~~ 10% of which suffered from dust storms or strong sandstorms. This event was considered to be the largest and strongest dust event to hit China in 2013. During this ~~processevent~~, suspended dust appeared in most of northwestern China, northern China, north and west Huanghuai region and west Liaoning province, ~~while the~~ west-central Inner Mongolia, west Gansu, northern Shanxi, and several parts of Xinjiang experienced a sandstorm. Along with the extreme dust event, there was a dramatic increase in PM_{10} , for example, the PM_{10} in Yulin, Shanxi even reached $10,000 \mu g \cdot m^{-3}$ (Wang et al., 2013; Zhang and Sun, 2013).

At 2 a.m. on March 10, ~~the~~ wind direction changed abruptly to northerly (see Fig. 8d) ~~and~~. ~~The the~~ scattering coefficient increased abruptly from $\sim 200 Mm^{-1}$ to $> 600 Mm^{-1}$ (~~see~~ Fig. 7b). PM_{10} mass concentrations at LinAn increased rapidly from $100 \mu g \cdot m^{-3}$ to $637 \mu g \cdot m^{-3}$, while the $PM_{2.5}$ mass concentration was only $190 \mu g \cdot m^{-3}$, accounting for 30% of PM_{10} . The Ångström exponent decreased from 1.2 to 0.8 (see Fig. 7c). All these phenomena implied the arrival of cold front from northern China enriched in coarse mode particles. The mass percentage of nitrate increased significantly and reached its peak ($\sim 26\%$) at 3 a.m.; meanwhile, the mass percentage

of OM decreased sharply from 2 a.m. to 3 a.m. (see Fig. 7e). Correspondingly, the scattering enhancement factor $f(85\%)$ reached 1.52 at 3 a.m. (see Fig. 7a), an increase of ~16% compared with that before the dust arrival. The most dust-dominated period, from 7 a.m. to 1 p.m., when the Ångström exponent was below 0.5 (Fig. 7c) and scattering coefficients at 450 nm, 550 nm and 700 nm (Fig. 7b) were ~~almost the same~~nearly equal, the scattering enhancement factor $f(85\%)$ was ~1.46. This value is much higher than the results ($f(80\%)=1.20$) reported by Pan et al. (2009) in rural Beijing, ($f(82.5\%)=1.18$) obtained by Carrico et al. (2003) in East Asia (ACE-Asia) during a dust episode, ($f(80\%)=1.20$) reported by Fierz-Schmidhauser et al. (2010) at a high alpine site (Jungfraujoch, 3580m a.s.l.) in Switzerland during a strong Saharan dust event, and ($f(80\%)=1.0-1.1$) measured by Li-Jones et al. (1998) in South America during an investigation of long-range transported Saharan dust. Meanwhile it is much lower than the value ($f(85\%)=1.73-2.20$) obtained by Kim et al. (2006) in Gosan (South Korea) during a dust-dominated period. According to Tobo et al. (2010), Ca-rich particles can react with gaseous HNO_3 to form $\text{Ca}(\text{NO}_3)_2$, thus the liquid cloud-nucleating ability would be enhanced. Similar results have also reported that aerosol hygroscopicity would be largely enhanced if coarse mode Ca-rich particles combined with nitrate (Shi et al., 2008; Sullivan et al., 2009). Thus, it is speculated that the relatively high $f(\text{RH})$ may have resulted from the reactions of coarse mode particles with inorganics (very likely to be nitrate) during long-range transport.

3.5 The relationship of scattering enhancement factor with chemical compositions

Scattering enhancement factor $f(85\%)$ versus organic mass fraction and inorganic mass fraction ~~were~~are shown in Fig. 8. The total mass concentration was calculated as the sum of mass concentrations of sulfate, nitrate, ammonium, chloride and organic measured by AMS and EBC measured by MAAP. The organic and inorganic mass fractions were calculated by dividing the mass concentration of organics (measured by AMS) and inorganics (the sum of sulfate, nitrate, ammonium and chloride measured by AMS) by the total mass concentration, respectively. The bivariate linear regression was applied with the uncertainty of $f(85\%, 550\text{nm})$ which was discussed in

Sect. 2.4 and the standard deviation of chemical compositions. The bivariate linear regressions (Fig. 8) clearly show ~~clearly~~ anti-correlation of $f(85\%, 550\text{nm})$ ~~to with the~~ organics fraction and strongly positive correlation of $f(85\%, 550\text{nm})$ to the inorganics fraction. This implies that chemical composition plays a vital role in aerosol hygroscopic properties. The absolute values of both slopes (1.2 for $f(85\%)$ vs. organic mass fraction and 0.96 for $f(85\%)$ vs. inorganic mass fraction) were much lower than those (3.1 and 2.2, respectively) measured at Melpitz, Germany (Zieger et al., 2014). This may partly ~~account be due~~ to the higher organic (or lower inorganic) contents at LinAn. Comparing Fig. 8 (a)(b) ~~and with~~ (c)(d), a ~~more clearly trend~~ stronger association of increasing nitrate with increasing $f(85\%)$ was observed. The role nitrate plays in aerosol hygroscopic properties will be discussed in the following paragraph.

$f(\text{RH})$ in Fig. 9 was expressed in terms of γ so as to be applied to a broader RH range (Doherty et al., 2005; Quinn et al., 2005): $\gamma = \ln f(\text{RH}) / \ln((100 - \text{RH}_{\text{ref}}) / (100 - \text{RH}))$. Here γ was based on $\text{RH}_{\text{ref}} = 40\%$ and $\text{RH} = 85\%$. The relative amount of OM and inorganics can be expressed as $F_o = C_o / (C_o + C_i)$, where C_o and C_i are the mass concentrations of OM and inorganics, respectively. Figure 9 shows γ versus F_o where C_i was the mass concentrations of SO_4^{2-} , NO_3^- and $\text{NO}_3^- + \text{SO}_4^{2-}$ in Fig. 9a, Fig. 9b and Fig. 9c, respectively. For all ~~the~~ three scatter plots, there is a trend of decreasing γ with increasing F_o . However, unlike the results of Quinn et al. (2005), Malm et al. (2005), Pan et al. (2009) and Yan et al. (2009), γ and F_o ($\text{OM} / (\text{OM} + \text{SO}_4^{2-})$) (~~shown in~~ Fig. 9a) were uncorrelated ($R^2 = 0.14$), while γ and F_o ($\text{OM} / (\text{OM} + \text{NO}_3^-)$) (~~shown in~~ Fig. 9b) and γ and F_o ($\text{OM} / (\text{OM} + \text{SO}_4^{2-} + \text{NO}_3^-)$) (~~shown in~~ Fig. 9c) were more strongly correlated (R^2 of 0.56 and 0.68, respectively). This result implies that NO_3^- ~~(rather played a stronger role in determining aerosol hygroscopic growth than SO_4^{2-})~~ ~~plays an important role in aerosol hygroscopic growth~~ during this study. This increasingly importance of nitrate corresponds to many recent studies in Shanghai (a mega city in Yangtze River Delta) (Shi et al., 2014) and Beijing (Sun et al., 2012). This may partly result from increasing availability of NH_3 to form NH_4NO_3 (Morgan et al., 2010) due to the decrease of SO_2 . The Chinese government has put an emphasis on the control of SO_2 emissions in recent years, ~~and The~~ desulfurization technology

~~were~~ has been installed at coal-fired power units as well as certain steel and cement production facilities, ~~as~~ As a result, the annual average concentration of SO_2 decreased significantly from 56 to $19 \mu\text{g}\cdot\text{m}^{-3}$ at LinAn from 2006 to 2012 (ZEPB, 2012; 2006).

The molar ratio of particulate SO_4^{2-} to total sulfur (SO_4^{2-} +gas phase SO_2) was used as an indicator of the relative age of aerosols (Quinn et al., 2005). For relatively younger aerosols, there is insufficient time for the conversion of SO_2 to SO_4^{2-} via gas and aqueous phase oxidation process and therefore the $\text{SO}_4^{2-}/(\text{SO}_4^{2-}+\text{SO}_2)$ molar ratio is low. As aerosol ages, more SO_2 is converted to SO_4^{2-} and thus the ratio increases. To illustrate the effects of this ratio and scattering coefficient on γ , Fig. 10 shows γ versus $\text{Fo}=\text{OM}/(\text{OM}+\text{SO}_4^{2-}+\text{NO}_3^-)$ colored by the $\text{SO}_4^{2-}/(\text{SO}_4^{2-}+\text{SO}_2)$ molar ratio (Fig. 10a) and $\log_{10}(\sigma_{\text{sp}})$ (Fig. 10b). The highest values of γ (~~or~~ $f(\text{RH})$) corresponded to more aged aerosols with a low OM content, ~~while~~ the lowest values corresponded to younger aerosols with a higher OM content, consistent with the result of Quinn et al. (2005). For aerosols with relatively low scattering coefficients, the value of $f(\text{RH})$ was usually low with a large variation (dots with cooler colors in Fig. 10b), ~~while~~ aerosols with high scattering coefficients ~~the~~ had values of $f(\text{RH})$ ~~was that were~~ relatively high with a small variation (dots with warm colors in Fig. 10b).

3.6 Parameterization of scattering enhancement factor $f(\text{RH})$

~~Scattering~~ The scattering enhancement factor $f(\text{RH})$ can be parameterized using with empirical equations (Kotchenruther and Hobbs, 1998; Kotchenruther et al., 1999; Gassó et al., 2000; Carrico et al., 2003; Liu et al., 2008; Pan et al., 2009; Zieger et al., 2010; Zieger et al., 2014). Humidograms ~~of from~~ LinAn were fitted ~~into~~ with two empirical equations and the fitting results ~~were~~ are shown below.

3.6.1 Parameterization with equation $f(\text{RH})=c(1-\text{RH})^{-g}$

Kasten (1969) proposed an empirical equation $f(\text{RH})=c(1-\text{RH})^{-g}$ to describe how $f(\text{RH})$ varies with RH, which has been used in previous reports e.g. by Kotchenruther and Hobbs (1998), Gassó et al. (2000), Carrico et al. (2003) and Zieger et al. (2010, 2014). Table 5 shows the fitting results ~~of from the current~~ this work and ~~other~~ previous studies. ~~The larger “c” and “g”, the~~ Larger $f(\text{RH})$ values are associated with

larger values of “c” and “g”. In this work, “g” was much lower than that in most of the other studies, ~~while-although it~~ was similar to the result of Gassó et al. (2000) during a dust episode. ~~It~~ The similarity results from the comparably low scattering enhancement factor (e.g. $f(80\%)=1.44\pm0.12$) ~~of-at~~ LinAn, which was similar to the value ($f(80\%)=1.33\pm0.07$) obtained by Gassó et al. (2000) for a dust event. The $f(RH)$ in other studies was much higher than that at LinAn, ranging from 2.04 (polluted marine aerosols in Gassó et al. (2000)) to 3.77 (arctic aerosols in Zieger et al. (2010)), therefore their parameter “g” was much higher.

3.6.2 Parameterization with equation $f(RH)=1+a \cdot RH^b$

The $f(RH)$ obtained at LinAn station can also be well described by the following equation, which was proposed by Kotchenruther and Hobbs (1998):

$$f(RH)=1+a \cdot RH^b \quad (5)$$

where “a” is positive and “b” is greater than 1. This function is convex, and has been used in many previous studies (Pan et al., 2009; ~~Delene and Ogren, 2002~~; Carrico et al., 2003; Kotchenruther et al., 1999; Kotchenruther and Hobbs, 1998) to describe monotonic growth. Theoretically, parameter “a” determines the largest value $f(100\%)$ can reach, and parameter “b” dominates the curvature of the function. The smaller “b” is, the smaller the curvature of humidogram will be; if “b” equals to 1, then $f(RH)=1+a \cdot RH$. The parameters “a” and “b” from our study and previous results for different aerosol types are listed in Table 6. Taking the locally-polluted episode as an example, although parameter “a” is slightly larger (~3%) than in the northerly-polluted episode, parameter “b” is ~40% larger, ~~;~~ as a result the $f(85\%)$ during locally-polluted period is smaller. Parameter “b” is ~~the-largestgreatest~~ in the locally-polluted episode, and smallest in the northerly-polluted period, i.e. the curvature of RH - $f(RH)$ line is largest during the locally-polluted episode, then is the dust episode, and the northerly-polluted period ~~is-the-smallest~~ shows the least curvature. These variations in curvature are, ~~which-is consistent-associated~~ with the mass percentages of nitrate, ~~as -will be discussed later (c.f. see Fig. 6) (will be discussed later).~~

3.6.3 Steepness of humidograms

~~Among~~ For all the humidograms measured at LinAn, $f(RH)$ increases continuously and monotonically. However, the curvatures of ~~different~~ the humidograms ~~are can be~~ different (Fig. 11); some increase with a nearly constant rate and the humidogram ~~line curve~~ is almost straight, while some increase slowly at first and then increase more steeply at relatively higher RH, thus the curvature of the humidogram is larger. In order to describe the growth pattern quantitatively, a steepness index η is defined based on the fitting curve:

$$\eta = f'(80\%) / f'(60\%) - 1 = (4/3)^{b-1} - 1 \quad (6)$$

where $f'(60\%)$ and $f'(80\%)$ represent the derivatives of the fitting curve at 60% and 80% RH, respectively. η is a nonnegative number. Zieger et al. (2010) has defined an index describing the magnitude of deliquescence transitions based on fitting equation $f(RH) = (1 - RH)^{-\eta}$ (see Sect. 3.6.1), while the steepness index η proposed in this study provided a way of quantitatively describing the steepness of humidograms ~~that are~~ well ~~fitted described into by the~~ equation $f(RH) = 1 + a RH^b$. The larger η is, the ~~bigger~~ ~~greater~~ the curvature. As is shown in Fig. 11a, for a large η , the $f'(60\%)$ is very small, meaning that aerosol scattering coefficient barely increases ($f(RH) \approx 1$) under low RH (usually $< 70\%$). Once reaching larger RH ($\sim 70\%$), $f(RH)$ begins to increase. However, for a small η (Fig. 11b), the difference of the derivatives at 60% and 80% RH was small, meaning the curvature of humidogram is much smaller.

A scatter plot of η and the mass percentage of nitrate is shown in Fig. 12, colored by the mass percentage of sulfate. As can be seen, η is negatively correlated with the mass percentage of nitrate. When the mass percentage of nitrate is below $\sim 18\%$, ~~the~~ ~~more nitrate, the smaller~~ η ~~decreases strongly as nitrate percentages increase is~~, which means ~~that~~ the humidogram line becomes straighter and the difference of the derivatives at lower and higher RHs becomes smaller. For a mass percentage of nitrate higher than 18% (correspondingly, a lower sulfate mass percentage), η is ~ 1.1 , meaning the humidogram line is almost straight (as shown in Fig. 11b) and aerosol scattering coefficient experiences a continuous and smooth growth at almost the same rate with RH.

3.7 Sensitivity of the direct radiative forcing of different aerosols to $f(RH)$

Direct radiative forcing of aerosols is quite sensitive to changes of relative humidity. The impact of relative humidity on globally-averaged, direct radiative forcing can be obtained by the following expression (Chylek and Wong, 1995):

$$\Delta F_R(RH) = -[S_0/4][T_a^2(1 - A_c)][2(1 - R_s)^2\bar{\beta}(RH)M\alpha_s f(RH) - 4R_s M\alpha_a] \quad (7)$$

where S_0 is the solar constant, T_a is the transmittance of the atmosphere above the aerosol layer, A_c is the fractional cloud amount, R_s is the albedo of the underlying surface, $\bar{\beta}(RH)$ is the solar radiation scattered back to space at defined RH, $f(RH)$ is the scattering enhancement factor, M is the column burden of aerosol (in g m^{-2}), α_s is the mass scattering efficiency, and α_a is the mass absorption efficiency.

In order to estimate the sensitivity of the forcing to different RHs for various aerosol types at LinAn (locally-polluted, northerly-polluted and dust-influenced aerosols), the ratio of direct aerosol radiative forcing ΔF_R at a defined RH to that at dry condition was calculated:

$$\frac{\Delta F_R(RH)}{\Delta F_R(\text{dry})} = \frac{(1 - R_s)^2\bar{\beta}(RH)\alpha_s f(RH) - 2R_s\alpha_a}{(1 - R_s)^2\bar{\beta}(\text{dry})\alpha_s f(\text{dry}) - 2R_s\alpha_a} \quad (8)$$

Parameters used in Eq. (8) were $R_s=0.15$, and $\alpha_a=0.3 \text{ m}^2\cdot\text{g}^{-1}$ (Wang et al., 2012; Hand and Malm, 2007). The mass scattering efficiency α_s is $2.76 \text{ m}^2\cdot\text{g}^{-1}$, which is derived from the slope of a linear regression of the measured scattering coefficients and the calculated PM_{10} mass concentrations based on TDMPS and APS measurement (see Fig. 13); the high mass scattering efficiency is explained by the high ratio of PM_1 to PM_{10} mass at this site (average 0.81). The average upscatter fraction $\bar{\beta}$ was calculated as $\bar{\beta}=0.0817+1.8495b-2.9682b^2$ (Delene and Ogren, 2002). The sensitivity of direct radiative forcing to RH for various aerosol types were-is shown in Fig. 14. As is shown in the figure, the variation of $\Delta F_R(RH)/\Delta F_R(\text{dry})$ with RH was-in accordance-with-corresponds to the variation of humidograms. The $f(RH)$ was-values were the largest during the northerly-polluted period, correspondingly, the effects of RH on aerosol radiative forcing during this period was the largest. The same was true for the locally-polluted period and the dust-influenced period. Since b decreases with increasing RH, this correspondence also demonstrates the vital role $f(RH)$ played in direct forcing enhancement. At 85% RH, the average ratio was 1.47, i.e. the direct

radiative forcing increased by 47% owing to the aerosol hygroscopicity.

Table 7 shows the mean influence of aerosol hygroscopicity on direct radiative forcing in March at LinAn. The ratios $\Delta F_R(RH_{amb})/\Delta F_R(dry)$ for locally-polluted, northerly-polluted and dust-influenced aerosols were calculated using the ambient average RH ($RH_{amb}=67\%$) in March at LinAn. The variables $f(RH_{amb})$, $b(RH_{amb})$, $\bar{\beta}(RH_{amb})$ and $\Delta F_R(RH_{amb})/\Delta F_R(dry)$ were the averages of the linear interpolation results of $f(RH)$, $b(RH)$, $\bar{\beta}(RH)$ and $\Delta F_R(RH)/\Delta F_R(dry)$ at 67% RH. The $\Delta F_R(RH_{amb})/\Delta F_R(dry)$ ratios were 1.118, 1.195 and 1.105, respectively (see Table 7). That is to say, on average, the direct radiative forcing of locally-polluted, northerly-polluted and dust-influenced aerosols increased by 11.8, 19.5 and 10.5% in March at LinAn.

4 Conclusions

The influence of aerosol water uptake on particles' aerosol light scattering properties and direct radiative forcing have been investigated at LinAn, a regional atmospheric background station in the Yangtze River Delta, China, using a scattering enhancement factor measurement system, together with AMS, MAAP and TDMPS providing the chemical composition and size distribution information. The average enhancement factors and mean standard deviations at 85% RH for scattering coefficient, backscattering coefficient and hemispheric backscatter fraction ($f(85\%)$, $f_b(85\%)$ and $f_{\beta}(85\%)$) were 1.58(0.12), 1.25(0.07) and 0.79(0.04), respectively. Slight A slight wavelength dependence of $f(85\%)$ was observed at higher $f(RH)$ values. Generally, the highest values of $f(RH)$ corresponded to aged aerosols with a small fraction of $OM_{\frac{1}{2}}$, while the lowest values corresponded to younger aerosols with a larger fraction of OM. $f(RH)$ of aerosols with relatively low scattering coefficients was usually low with a large variation; while $f(RH)$ of aerosols with high scattering coefficients was relatively high with a small variation. Besides, Nitrate was found to NO_3^- plays an important role in determining the magnitude of $f(RH)$ at LinAn.

Humidograms measured at LinAn can be well described by the two equations: $f(RH)=c(1-RH)^{-d}$ and $f(RH)=1+aRH^b$. Further investigation shows the

shape of the humidogram is closely related to the mass percentage of nitrate. A steepness index η has been defined to quantitatively determine the steepness of the humidograms. The least curvature of the humidograms (smallest η) was associated with the highest more-nitrate mass fractions (or and less-lowest sulfate fractions), the smaller η is and the straighter the curve will be. In March, the average relative humidity (RH_{amb}) was 67%. Consequently, the direct radiative forcing of locally-polluted, northerly-polluted and dust-influenced aerosols increased by 11.8, 19.5 and 10.5%, respectively due to aerosol uptake water in March at LinAn. At 85% RH, the direct radiative forcing increased by as high-much as 47% due to ~~the~~-aerosol hygroscopicity. In conclusion, water plays an important role in aerosol scattering properties as well as the radiative forcing, and it should be paid high careful attention to humidity effects is required when comparing ~~between~~-remote sensing and in-situ measurements and-or calculating the climate forcing.

Acknowledgments: This work was supported by National Basic Research Program of China (2011CB403401), the National Natural Science Foundation of China (41475118, 41175113), China International Science and Technology Cooperation Project (2009DFA22800), CAMS Basis Research Project (2013Z007, 2013Y004), and the Meteorological Special Project of China (GYHY-200906038, GYHY201206037). This paper is partially supported by the CMA Innovation Team for Haze-fog Observation and Forecasts. The authors would also like to thank the LinAn observational station staff for their support. The authors would thank Dr. D. Covert of University of Washington Seattle Department of Atmospheric Sciences USA for useful discussions.

References

Ackerman, A. S., Kirkpatrick, M. P., Stevens, D. E., and Toon, O. B.: The impact of humidity above stratiform clouds on indirect aerosol climate forcing, *Nature*, 432, 1014-1017, 2004.

- Adam, M., Putaud, J., Martins dos Santos, S., Dell'Acqua, A., and Gruening, C.: Aerosol hygroscopicity at a regional background site (Ispra) in Northern Italy, *Atmos. Chem. Phys.*, 12, 5703-5717, 2012.
- Anderson, T., Covert, D., Marshall, S., Laucks, M., Charlson, R., Waggoner, A., Ogren, J., Caldow, R., Holm, R., and Quant, F.: Performance characteristics of a high-sensitivity, three-wavelength, total scatter/backscatter nephelometer, *J. Atmos. Ocean. Tech.*, 13, 967-986, 1996.
- Anderson, T. L., and Ogren, J. A.: Determining aerosol radiative properties using the TSI 3563 integrating nephelometer, *Aerosol Sci. Tech.*, 29, 57-69, 1998.
- Berner, A., Lürzer, C., Pohl, F., Preining, O., and Wagner, P.: The size distribution of the urban aerosol in Vienna, *Sci. Total Environ.*, 13, 245-261, 1979.
- Birmili, W., Stratmann, F., and Wiedensohler, A.: Design of a DMA-based size spectrometer for a large particle size range and stable operation, *J. Aerosol Sci.*, 30, 549-553, 1999.
- Carrico, C. M., Rood, M. J., and Ogren, J. A.: Aerosol light scattering properties at Cape Grim, Tasmania, during the first Aerosol Characterization Experiment (ACE 1), *J. Geophys. Res.*, 103, 16565-16574, 1998.
- Carrico, C. M., Rood, M. J., Ogren, J. A., Neusüß, C., Wiedensohler, A., and Heintzenberg, J.: Aerosol Optical properties at Sagres, Portugal during ACE-2, *Tellus B*, 52, 694-715, 2000.
- Carrico, C. M., Kus, P., Rood, M. J., Quinn, P. K., and Bates, T. S.: Mixtures of pollution, dust, sea salt, and volcanic aerosol during ACE-Asia: Radiative properties as a function of relative humidity, *J. Geophys. Res.*, 108, 8650, 10.1029/2003JD003405, 2003.
- Charlson, R.J., Ahlquist, N., Selvidge, H., and MacCready Jr, P.: Monitoring of atmospheric aerosol parameters with the integrating nephelometer, *JAPCA J. Air Waste Ma.*, 19, 937-942, 1969.
- Charlson, R. J., Schwartz, S., Hales, J., Cess, R. D., Coakley Jr, J. A., Hansen, J., and Hofmann, D.: Climate forcing by anthropogenic aerosols, *Science*, 255, 423-430, 1992.
- Cheng, Y., Wiedensohler, A., Eichler, H., Heintzenberg, J., Tesche, M., Ansmann, A., Wendisch, M., Su, H., Althausen, D., and Herrmann, H.: Relative humidity dependence of aerosol optical properties and direct radiative forcing in the surface boundary layer at Xinken in Pearl River Delta of China: An observation based numerical study, *Atmos. Environ.*, 42, 6373-6397, 2008.
- Chylek, P., and Wong, J.: Effect of absorbing aerosols on global radiation budget, *Geophys. Res. Lett.*, 22, 929-931, 1995.
- Covert, D. S., Charlson, R., and Ahlquist, N.: A study of the relationship of chemical composition and humidity to light scattering by aerosols, *J. Appl. Meteorol.*, 11, 968-976, 1972.
- Day, D. E., and Malm, W. C.: Aerosol light scattering measurements as a function of relative humidity: a comparison between measurements made at three different sites, *Atmos. Environ.*, 35, 5169-5176, 2001.
- Delene, D. J., and Ogren, J. A.: Variability of aerosol optical properties at four North American surface monitoring sites, *J. Atmos. Sci.*, 59, 1135-1150, 2002.
- Dick, W. D., Saxena, P., and McMurtry, P. H.: Estimation of water uptake by organic compounds in submicron aerosols measured during the Southeastern Aerosol and Visibility Study, *J. Geophys. Res.-Atmos.*, 105, 1471-1479, 2000.
- Doherty, S. J., Quinn, P. K., Jefferson, A., Carrico, C. M., Anderson, T. L., and Hegg, D.: A comparison and summary of aerosol optical properties as observed in situ from aircraft, ship, and land during ACE-Asia, *J. Geophys. Res.*, 110, D04201, doi: 10.1029/2004JD004964, 2005.
- Engelhart, G., Hildebrandt, L., Kostenidou, E., Mihalopoulos, N., Donahue, N., and Pandis, S.: Water content of aged aerosol, *Atmos. Chem. Phys.*, 11, 911-920, 2011.

727 Fang, S. X., Zhou, L. X., Masarie, K. A., Xu, L., and Rella, C. W.: Study of atmospheric CH₄ mole fractions
 728 at three WMO/GAW stations in China, *J. Geophys. Res.-Atmos.*, 118, 4874-4886, 2013.
 729 Fierz-Schmidhauser, R., Zieger, P., Gysel, M., Kammermann, L., DeCarlo, P., Baltensperger, U., and
 730 Weingartner, E.: Measured and predicted aerosol light scattering enhancement factors at the high
 731 alpine site Jungfraujoch, *Atmos. Chem. Phys.*, 10, 2319-2333, 2010.
 732 Gasso, S., Hegg, D., Covert, D., Collins, D., Noone, K., Öström, E., Schmid, B., Russell, P., Livingston, J.,
 733 and Durkee, P.: Influence of humidity on the aerosol scattering coefficient and its effect on the
 734 upwelling radiance during ACE-2, *Tellus B*, 52, 546-567, 2000.
 735 Hänel, G.: The properties of atmospheric aerosol particles as functions of the relative humidity at
 736 thermodynamic equilibrium with the surrounding moist air, *Adv. Geophys.*, 19, 73-188, 1976.
 737 Hand, J., and Malm, W.: Review of aerosol mass scattering efficiencies from ground-based
 738 measurements since 1990, *J. Geophys. Res.-Atmos.*, 112, D16203, doi:10.1029/2007JD008484,
 739 2007.
 740 Kim, J., Yoon, S.-C., Jefferson, A., and Kim, S.-W.: Aerosol hygroscopic properties during Asian dust,
 741 pollution, and biomass burning episodes at Gosan, Korea in April 2001, *Atmos. Environ.*, 40,
 742 1550-1560, 2006.
 743 Koloutsou-Vakakis, S., Carrico, C., Kus, P., Rood, M., Li, Z., Shrestha, R., Ogren, J., Chow, J., and Watson,
 744 J.: Aerosol properties at a midlatitude Northern Hemisphere continental site, *J. Geophys. Res.*, 106,
 745 3019-3032, 2001.
 746 Kotchenruther, R. A. and Hobbs, P. V.: Humidification factors of aerosols from biomass burning in
 747 Brazil, *J. Geophys. Res.*, 103, 32081-32089, doi: 10.1029/98jd00340, 1998.
 748 Kotchenruther, R. A., Hobbs, P. V., and Hegg, D. A.: Humidification factors for atmospheric aerosols off
 749 the mid-Atlantic coast of the United States, *J. Geophys. Res.*, 104, 2239-2251, 1999.
 750 Li-Jones, X., Maring, H. B., and Prospero, J. M.: Effect of relative humidity on light scattering by mineral
 751 dust aerosol as measured in the marine boundary layer over the tropical Atlantic Ocean, *J. Geophys.*
 752 *Res.*, 103, 31113-31121, 1998.
 753 Liu, X., Zhang, Y., Jung, J., Gu, J., Li, Y., Guo, S., Chang, S.-Y., Yue, D., Lin, P., Kim, Y. J., Hu, M., Zeng, L.,
 754 and Zhu, T.: Research on the hygroscopic properties of aerosols by measurement and modeling
 755 during CAREBeijing-2006, *J. Geophys. Res.-Atmos.*, 114, D00G16, doi: 10.1029/2008JD010805, 2009.
 756 Magi, B. I., and Hobbs, P. V.: Effects of humidity on aerosols in southern Africa during the biomass
 757 burning season, *J. Geophys. Res.-Atmos.* 108, 8504, doi:10.1029/2002JD002144, 2003.
 758 Malm, W. C., and Day, D. E.: Optical properties of aerosols at Grand Canyon national park, *Atmos.*
 759 *Environ.*, 34, 3373-3391, 2000.
 760 Malm, W. C., and Day, D. E.: Estimates of aerosol species scattering characteristics as a function of
 761 relative humidity, *Atmos. Environ.*, 35, 2845-2860, 2001.
 762 Malm, W. C., Day, D. E., Kreidenweis, S. M., Collett, J. L., and Lee, T.: Humidity-dependent optical
 763 properties of fine particles during the Big Bend Regional Aerosol and Visibility Observational Study, *J.*
 764 *Geophys. Res.*, 108, 4279, doi:10.1029/2002JD002998, 2003.
 765 Malm, W. C., Day, D. E., Kreidenweis, S. M., Collett, J. L., Carrico, C., McMeeking, G., and Lee, T.:
 766 Hygroscopic properties of an organic-laden aerosol, *Atmos. Environ.*, 39, 4969-4982, 2005.
 767 Meng, Z. Y., Jia, X. F., Zhang, R. J., Yu, X. M., and Ma, Q. L.: Characteristics of PM_{2.5} at Lin'an Regional
 768 Background Station in the Yangtze River Delta Region, *J. Appl. Meteorol. Sci.*, 23, 424-432, 2012.
 769 Morgan, W., Allan, J., Bower, K., Esselborn, M., Harris, B., Henzing, J., Highwood, E., Kiendler-Scharr, A.,
 770 McMeeking, G., and Mensah, A.: Enhancement of the aerosol direct radiative effect by

771 semi-volatile aerosol components: airborne measurements in North-Western Europe, *Atmos. Chem.*
772 *Phys.*, 10, 8151-8171, 2010.

773 Müller T., Laborde M., Kassell G., and Wiedensohler A., Design and performance of a three wavelength
774 LED-based total scatter and backscatter integrating nephelometer, *Atmos. Meas. Tech.*, 4(6), 1291–
775 1303, doi:10.5194/amt-4-1291-2011, 2011.

776 Pan, L., Che, H., Geng, F., Xia, X., Wang, Y., Zhu, C., Chen, M., Gao, W., and Guo, J.: Aerosol optical
777 properties based on ground measurements over the Chinese Yangtze Delta Region, *Atmos. Environ.*,
778 44, 2587-2596, 2010.

779 Pan, X. L., Yan, P., Tang, J., Ma, J., Wang, Z., Gbaguidi, A., and Sun, Y.: Observational study of influence
780 of aerosol hygroscopic growth on scattering coefficient over rural area near Beijing mega-city,
781 *Atmos. Chem. Phys.*, 9, 7519-7530, 2009.

782 Pilinis, C., Seinfeld, J. H., and Grosjean, D.: Water content of atmospheric aerosols, *Atmos. Environ.*, 23,
783 1601-1606, 1989.

784 Pilinis, C., Pandis, S. N., and Seinfeld, J. H.: Sensitivity of direct climate forcing by atmospheric aerosols
785 to aerosol size and composition, *J. Geophys. Res.*, 100, 18739-18754, 1995.

786 Qi, H., Lin, W., Xu, X., Yu, X., and Ma, Q.: Significant downward trend of SO₂ observed from 2005 to
787 2010 at a background station in the Yangtze Delta region, China, *Sci. China Ser. B*, 55, 1451-1458,
788 2012.

789 Quinn, P., Marshall, S., Bates, T., Covert, D., and Kapustin, V.: Comparison of measured and calculated
790 aerosol properties relevant to the direct radiative forcing of tropospheric sulfate aerosol on climate,
791 *J. Geophys. Res.*, 100, 8977-8991, 1995.

792 Quinn, P. K., Bates, T. S., Baynard, T., Clarke, A. D., Onasch, T. B., Wang, W., Rood, M. J., Andrews, E.,
793 Allan, J., Carrico, C. M., Coffman, D., and Worsnop, D.: Impact of particulate organic matter on the
794 relative humidity dependence of light scattering: A simplified parameterization, *Geophys. Res. Lett.*,
795 32, L22809, doi: 10.1029/2005gl024322, 2005.

796 Randles, C., Russell, L., and Ramaswamy, V.: Hygroscopic and optical properties of organic sea salt
797 aerosol and consequences for climate forcing, *Geophys. Res. Lett.*, 31, L16108,
798 doi:10.1029/2004GL020628, 2004.

799 Shen, X., Sun, J., Zhang, Y., Wehner, B., Nowak, A., Tuch, T., Zhang, X., Wang, T., Zhou, H., and Zhang, X.:
800 First long-term study of particle number size distributions and new particle formation events of
801 regional aerosol in the North China Plain, *Atmos. Chem. Phys.*, 11, 1565-1580,
802 doi:10.5194/acp-11-1565-2011, 2011.

803 Shi, Y., Chen, J., Hu, D., Wang, L., Yang, X., and Wang, X.: Airborne submicron particulate (PM₁)
804 pollution in Shanghai, China: Chemical variability, formation/dissociation of associated
805 semi-volatile components and the impacts on visibility, *Sci. Total Environ.*, 473, 199-206, 2014.

806 Shi, Z., Zhang, D., Hayashi, M., Ogata, H., Ji, H., and Fujiie, W.: Influences of sulfate and nitrate on the
807 hygroscopic behaviour of coarse dust particles, *Atmos. Environ.*, 42, 822-827, 2008.

808 Sjogren, S., Gysel, M., Weingartner, E., Baltensperger, U., Cubison, M., Coe, H., Zardini, A., Marcolli, C.,
809 Krieger, U., and Peter, T.: Hygroscopic growth and water uptake kinetics of two-phase aerosol
810 particles consisting of ammonium sulfate, adipic and humic acid mixtures, *J. Aerosol Sci.*, 38,
811 157-171, 2007.

812 Sullivan, R., Moore, M., Petters, M., Kreidenweis, S., Roberts, G., and Prather, K.: Effect of chemical
813 mixing state on the hygroscopicity and cloud nucleation properties of calcium mineral dust particles,
814 *Atmos. Chem. Phys.*, 9, 3303-3316, 2009.

815 Sun, J., Zhang, Q., Canagaratna, M. R., Zhang, Y., Ng, N. L., Sun, Y., Jayne, J. T., Zhang, X., Zhang, X., and
816 Worsnop, D. R.: Highly time- and size-resolved characterization of submicron aerosol particles in
817 Beijing using an Aerodyne Aerosol Mass Spectrometer, *Atmos. Environ.*, 44, 131-140, 2010.

818 Sun, Y., Wang, Z., Dong, H., Yang, T., Li, J., Pan, X., Chen, P., and Jayne, J. T.: Characterization of summer
819 organic and inorganic aerosols in Beijing, China with an Aerosol Chemical Speciation Monitor,
820 *Atmos. Environ.*, 51, 250-259, 2012.

821 Tang, I. N.: Chemical and size effects of hygroscopic aerosols on light scattering coefficients, *J. Geophys.*
822 *Res.-Atmos.*, 101, 19245-19250, 1996.

823 Tobo, Y., Zhang, D., Matsuki, A., and Iwasaka, Y.: Asian dust particles converted into aqueous droplets
824 under remote marine atmospheric conditions, *P. Natl. Acad. Sci. USA*, 107, 17905-17910, 2010.

825 Tuch, T. M., Haudek, A., Müller, T., Nowak, A., Wex, H., and Wiedensohler, A.: Design and performance
826 of an automatic regenerating adsorption aerosol dryer for continuous operation at monitoring sites,
827 *Atmos. Meas. Tech.*, 2, 417-422, doi:10.5194/amt-2-417-2009, 2009.

828 Wang, Y., Zhang, X., and Draxler, R. R.: TrajStat: GIS-based software that uses various trajectory
829 statistical analysis methods to identify potential sources from long-term air pollution measurement
830 data, *Environ. Modell. Softw.*, 24, 938-939, 2009.

831 Wang, J. and Martin, S. T.: Satellite characterization of urban aerosols: Importance of including
832 hygroscopicity and mixing state in the retrieval algorithms, *J. Geophys. Res.-Atmos.*, 112, D17203,
833 doi:10.1029/2006JD008078, 2007.

834 Wang, M. X., Ding, X., Fu, X., He, Q., Wang, S., Bernard, F., Zhao, X., and Wu, D.: Aerosol scattering
835 coefficients and major chemical compositions of fine particles observed at a rural site in the central
836 Pearl River Delta, South China, *J. Environ. Sci.*, 24, 72-77, 2012.

837 Wang, L. P., Zhang, B. H., and Zhang, X. W.: Main weather processes in March and April, 2013, *Weather*
838 *Forecast Rev.*, 5, 1-7, 2013.

839 Weingartner, E., Baltensperger, U., and Burtscher, H.: Growth and structural change of combustion
840 aerosols at high relative humidity, *Environ. Sci. Technol.*, 29, 2982-2986, 1995.

841 Wiscombe, W., and Grams, G.: The backscattered fraction in two-stream approximations, *J. Atmos. Sci.*,
842 33, 2440-2451, 1976.

843 Xu, J., Bergin, M., Yu, X., Liu, G., Zhao, J., Carrico, C., and Baumann, K.: Measurement of aerosol
844 chemical, physical and radiative properties in the Yangtze delta region of China, *Atmos. Environ.*, 36,
845 161-173, 2002.

846 Xu, X., Lin, W., Wang, T., Yan, P., Tang, J., Meng, Z., and Wang, Y.: Long-term trend of surface ozone at a
847 regional background station in eastern China 1991-2006: enhanced variability, *Atmos. Chem. Phys.*,
848 8, 2595-2607, doi:10.5194/acp-8-2595-2008, 2008.

849 Yan, P., Zhang, Y. M., Yang, D. Z., Tang, J., Yu, X. L., Cheng, H. B., and Yu, X. M.: The characteristic of
850 aerosol ionic size distributions at Lin'an in summer of 2003, *Acta Meteor. Sin.*, 63, 980-987, 2005.

851 Yan, P., Pan, X., Tang, J., Zhou, X., Zhang, R., and Zeng, L.: Hygroscopic growth of aerosol scattering
852 coefficient: A comparative analysis between urban and suburban sites at winter in Beijing,
853 *Particuology*, 7, 52-60, 2009.

854 Zhang, B. and Sun, J.: Analysis of the March 2013 atmospheric circulation and Weather, *Meteor. Mon.*,
855 39, 794-800, 2013.

856 Zhang, Y. Y., Zuo, L. F., Ren, X. C., and Cui, J.: Research of the aerosol scattering properties based on
857 evaporation duct, *Ship Electron. Eng.*, 32, 12-14, 2012.

858 Zhejiang Environmental Protection Bureau (ZEPB), 1999, Annual Report on the State of the

Environment of Zhejiang Province, Zhejiang Environmental Protection Bureau, Hangzhou, 1999.

Zhejiang Environmental Protection Bureau (ZEPB), 2006, Annual Report on the State of the Environment of Zhejiang Province, Zhejiang Environmental Protection Bureau, Hangzhou, 21 pp., 2006.

Zhejiang Environmental Protection Bureau (ZEPB), 2012, Annual Report on the State of the Environment of Zhejiang Province, Zhejiang Environmental Protection Bureau, Hangzhou, 29 pp., 2012.

Zhejiang Environmental Protection Bureau (ZEPB), 2013, Annual Report on the State of the Environment of Zhejiang Province, Zhejiang Environmental Protection Bureau, Hangzhou, 33 pp., 2013.

Zieger, P., Fierz-Schmidhauser, R., Gysel, M., Ström, J., Henne, S., Yttri, K. E., Baltensperger, U., and Weingartner, E.: Effects of relative humidity on aerosol light scattering in the Arctic, *Atmos. Chem. Phys.*, 10, 3875-3890, doi:10.5194/acp-10-3875-2010, 2010.

Zieger, P., Weingartner, E., Henzing, J., Moerman, M., Leeuw, G. d., Mikkilä, J., Ehn, M., Petäjä, T., Clémer, K., and Roozendaal, M. v.: Comparison of ambient aerosol extinction coefficients obtained from in-situ, MAX-DOAS and LIDAR measurements at Cabauw, *Atmos. Chem. Phys.*, 11, 2603-2624, doi:10.5194/acp-11-2603-2011, 2011.

Zieger, P., Kienast-Sjögren, E., Starace, M., Bismarck, J. v., Bukowiecki, N., Baltensperger, U., Wienhold, F., Peter, T., Ruhtz, T., and Collaud Coen, M.: Spatial variation of aerosol optical properties around the high-alpine site Jungfraujoch (3580 m asl), *Atmos. Chem. Phys.*, 12, 7231-7249, doi:10.5194/acp-12-7231-2012, 2012.

Zieger, P., Fierz-Schmidhauser, R., Weingartner, E., and Baltensperger, U.: Effects of relative humidity on aerosol light scattering: results from different European sites, *Atmos. Chem. Phys.*, 13, 10609-10631, doi:10.5194/acp-13-10609-2013, 2013.

Zieger, P., Fierz-Schmidhauser, R., Poulain, L., Müller, T., Birmili, W., Spindler, G., Wiedensohler, A., Baltensperger, U., and Weingartner, E.: Influence of water uptake on the aerosol particle light scattering coefficients of the Central European aerosol, *Tellus B*, 66, 22716, doi:10.3402/tellusb.v66.22716, 2014.

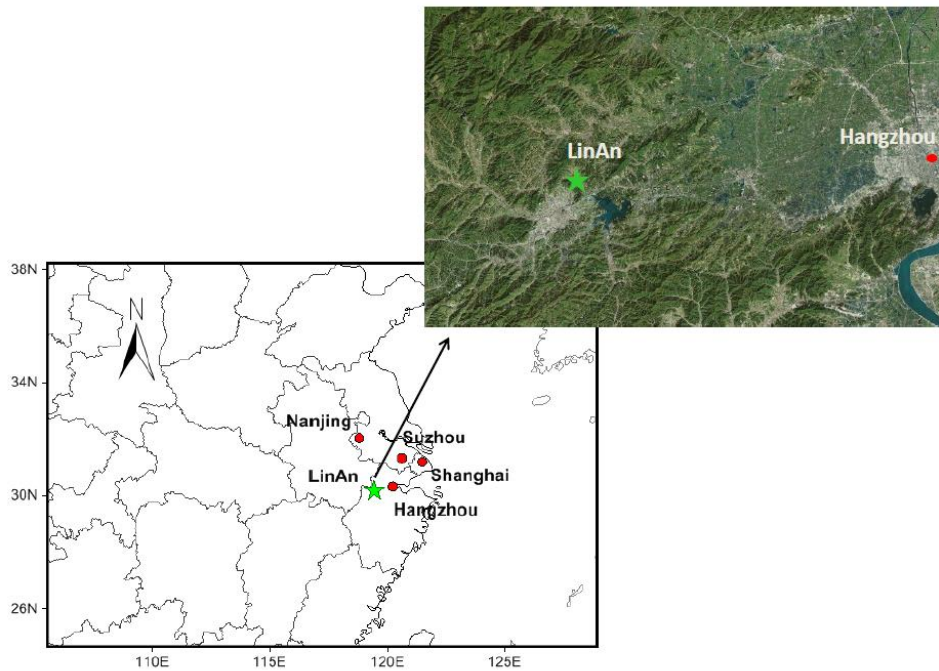


Fig. 1 Location of LinAn station (green star) and the main cities in the Yangtze River Delta (red dots) in the lower left panel. The upper right panel ~~is~~ shows the topography of the surrounding area.

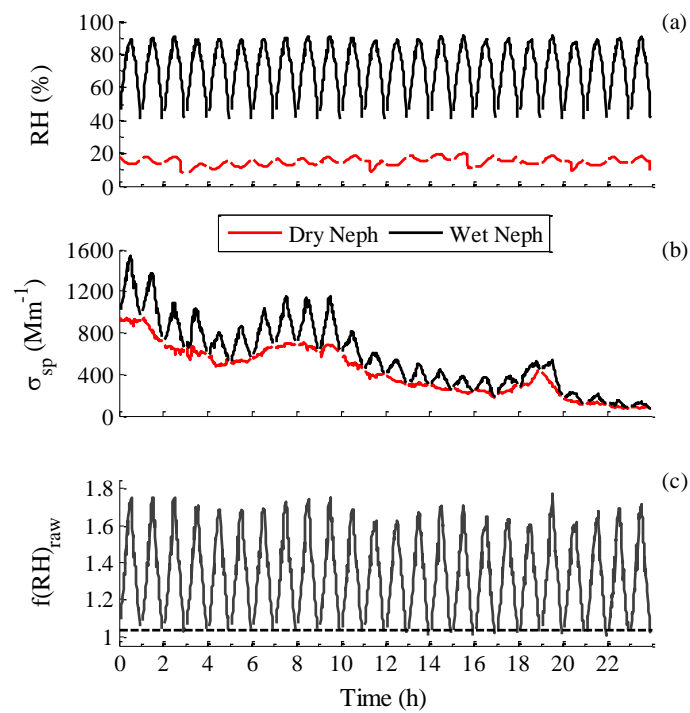


Fig. 2 Example of ~~recorded-measured~~ data on 17 March 2013 (a) Relative humidity inside DryNeph (red line) and WetNeph (black line); (b) Aerosol scattering

coefficients measured by DryNeph (red line) and WetNeph (black line) at 550nm wavelength; (c) Raw scattering enhancement factor $f(\text{RH}, 550\text{nm})_{\text{raw}}$ without normalization, the black dashed line was at $f(\text{RH})_{\text{raw}}=1.03$.

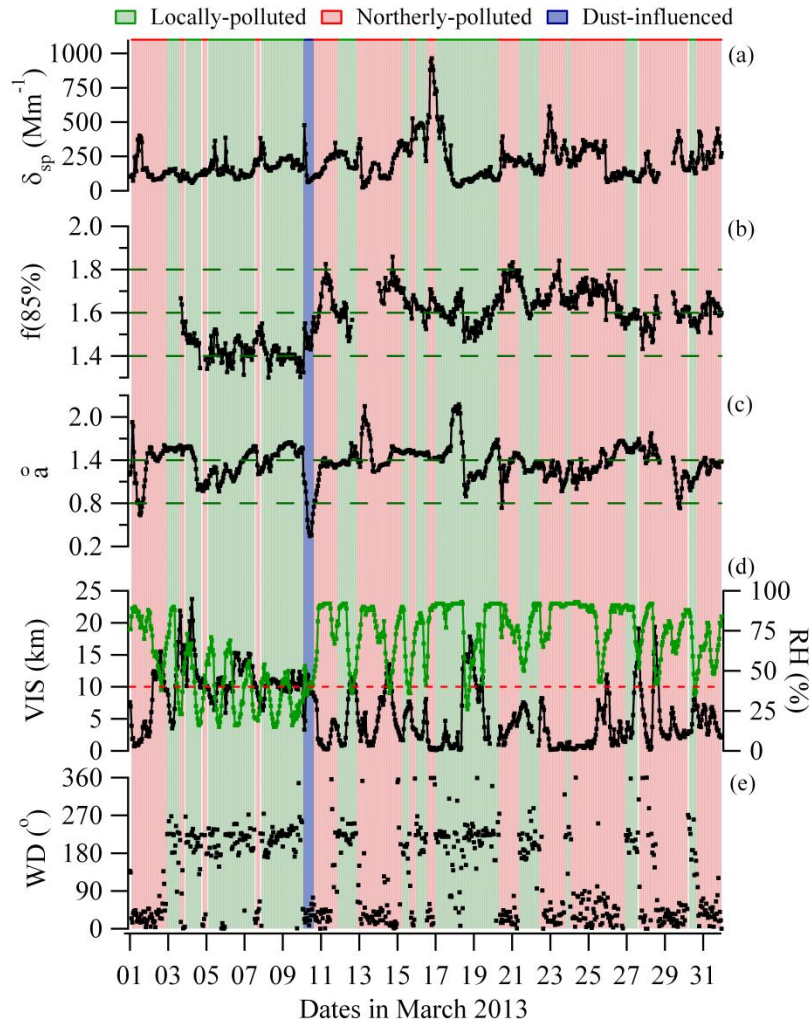
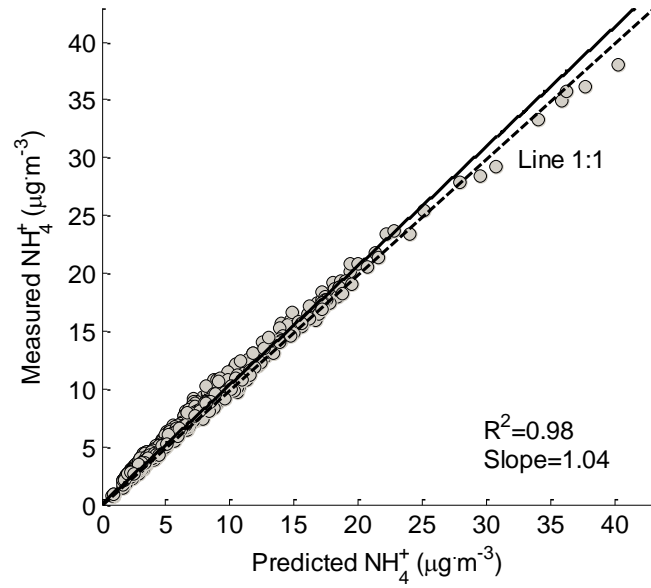


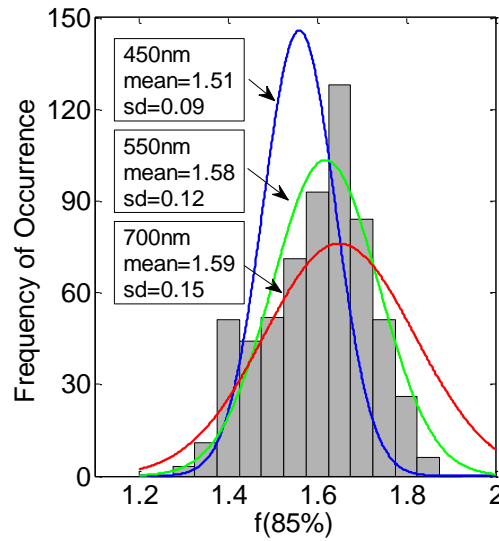
Fig. 3 Time series of measured and derived aerosol variables, as well as the ambient RH and visibility. (a) Aerosol scattering coefficient of DryNeph at 550 nm wavelength; scattering enhancement factor $f(85\%)$ at 550 nm wavelength; (b) scattering enhancement factor $f(85\%)$ at 550 nm wavelength; visibility (VIS) and relative humidity (RH) at ambient conditions, the dashed line represents $\text{VIS}=10$ km; (c) Ångström exponent \AA aerosol scattering coefficient of DryNeph at 550 nm wavelength; (d) visibility (VIS) and relative humidity (RH) at ambient conditions, the red dashed line represents $\text{VIS}=10$ km; Ångström exponent \AA (e) wind direction (WD), indicating that prevailing wind directions during the observation period was were

908 mainly northeasterly (NE) and southwesterly (SW).



909

910 Fig. 4 Measured and predicted mass concentration of ammonium. The predicted mass
 911 concentration of ammonium (NH_4^+ _{predicted}) is calculated by Eq. (4). The solid black
 912 line represents the linear least square regression.



913

914 Fig. 5 Histograms of $f(85\%, 550 \text{ nm})$ overlaid with the Gaussian curves based on the
 915 statistics for $f(85\%, 450 \text{ nm})$, $f(85\%, 550 \text{ nm})$ and $f(85\%, 700 \text{ nm})$.

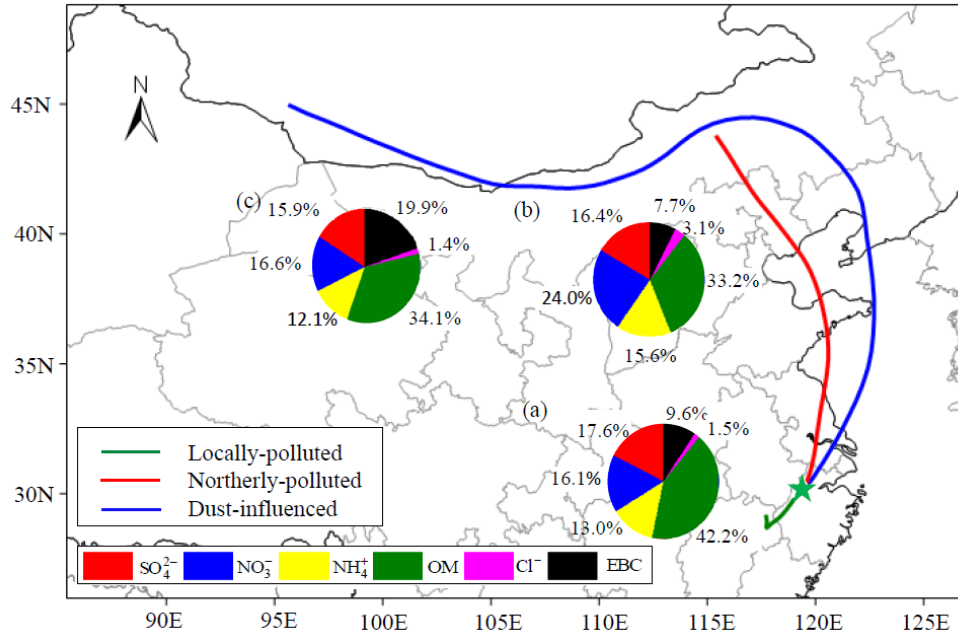


Fig. 6 72h back trajectories of locally-polluted periods, northerly-polluted periods and dust-influenced period, together with the mean mass fractions of submicron chemical compositions-species (SO₄²⁻, NO₃⁻, NH₄⁺, OM and Cl⁻) measured by AMS and EBC in PM₁₀ measured by MAAP. The pie charts (a), (b) and (c) were for locally-polluted, northerly-polluted and dust-influenced periods, respectively.

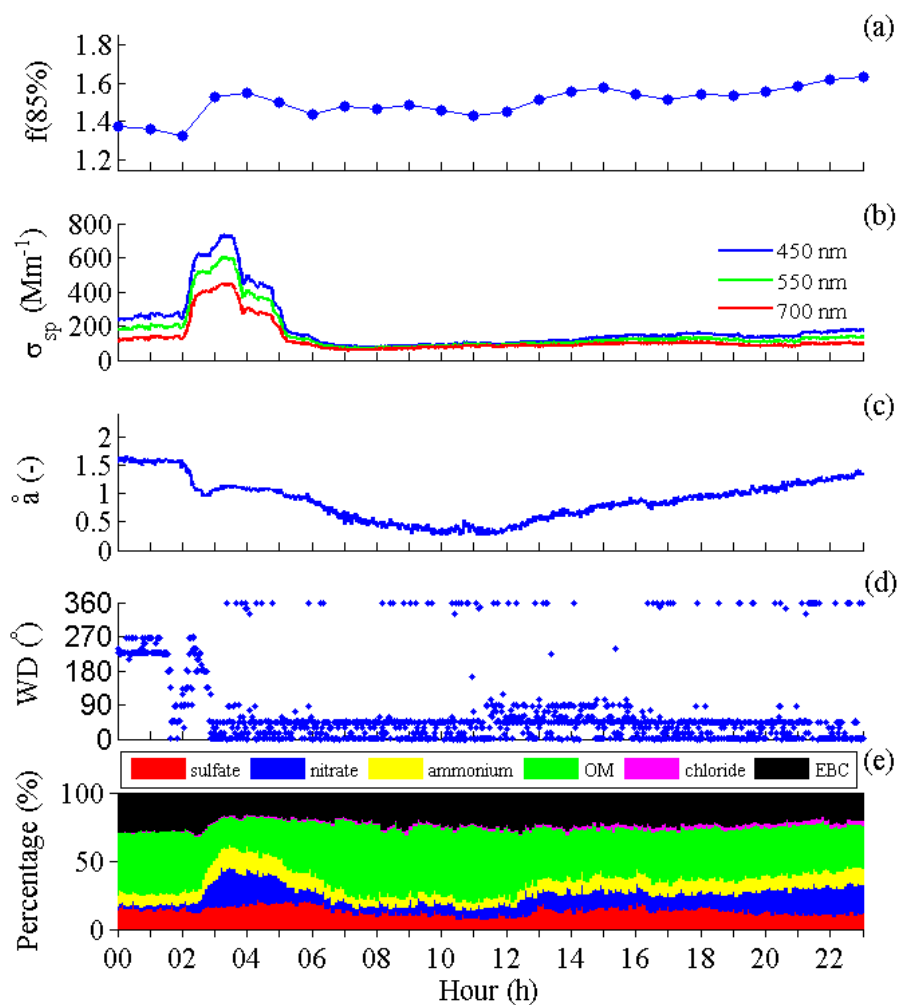


Fig. 7 Parameters in episode influenced by dust on 10 March 2013 at LinAn (a) scattering enhancement factor $f(85\%)$ at 550nm wavelength; (b) scattering coefficients at 450nm, 550nm and 700nm wavelengths; (c) Ångström exponent \tilde{a} (d) wind direction; (e) mass percentages of chemical species measured by AMS and MAAP.

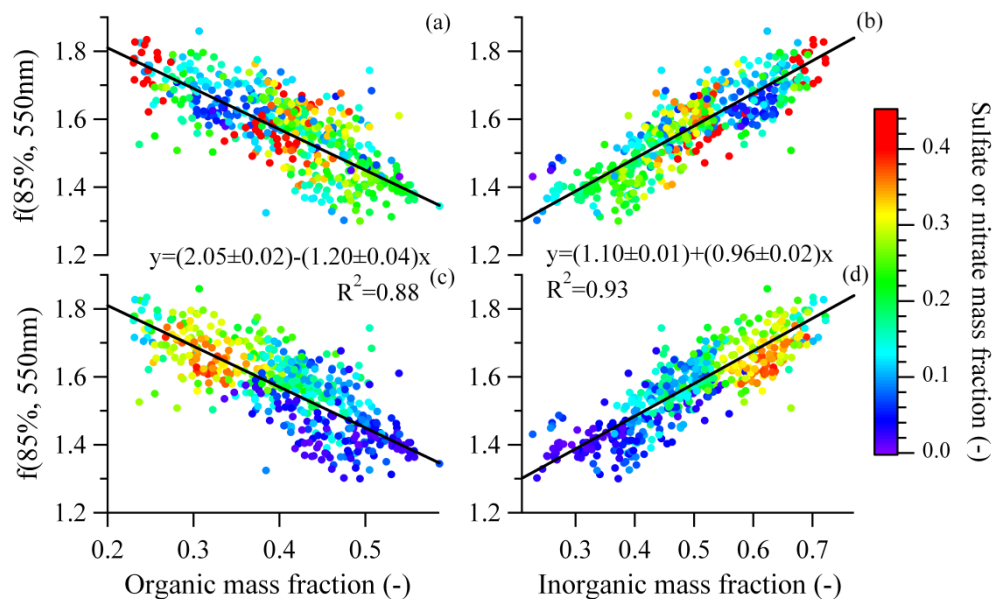


Fig. 8 Scattering enhancement factor $f(85\%, 550\text{nm})$ vs. organic mass fraction and inorganic mass fraction determined from AMS and MAAP: (a) (b) $f(85\%, 550\text{nm})$ vs. organic mass and inorganic mass fraction colored by sulfate mass fraction, respectively; (c) (d) $f(85\%, 550\text{nm})$ vs. organic mass fraction and inorganic mass fraction colored by nitrate mass fraction, respectively. The solid black line represent a bivariate linear regression including the uncertainty of $f(85\%, 550\text{nm})$ and the standard deviation of chemical compositions.

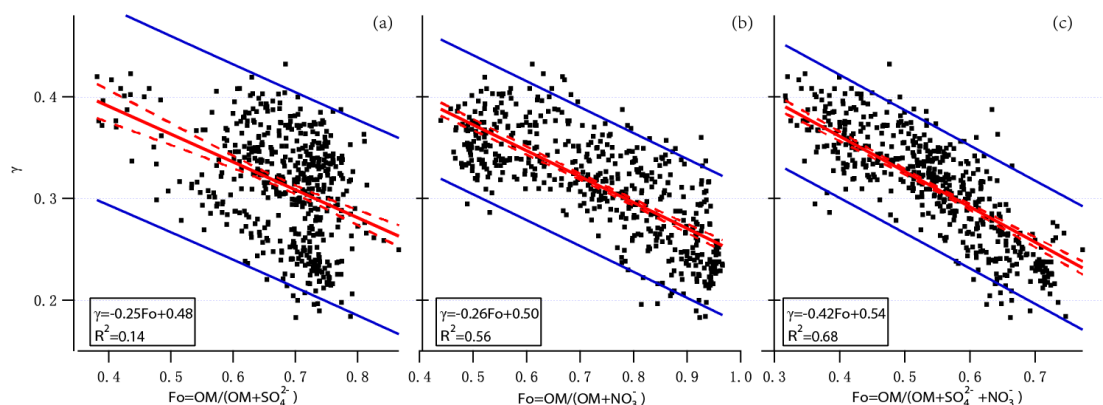


Fig. 9 scatter plots of γ versus Fo (a) $Fo = OM/(OM + SO_4^{2-})$, (b) $Fo = OM/(OM + NO_3^-)$ and (c) $Fo = OM/(OM + SO_4^{2-} + NO_3^-)$. Solid red lines represent the linear fit, dashed red lines show the 95% confidence level for the fit, and solid blue lines show the 95% prediction bands.

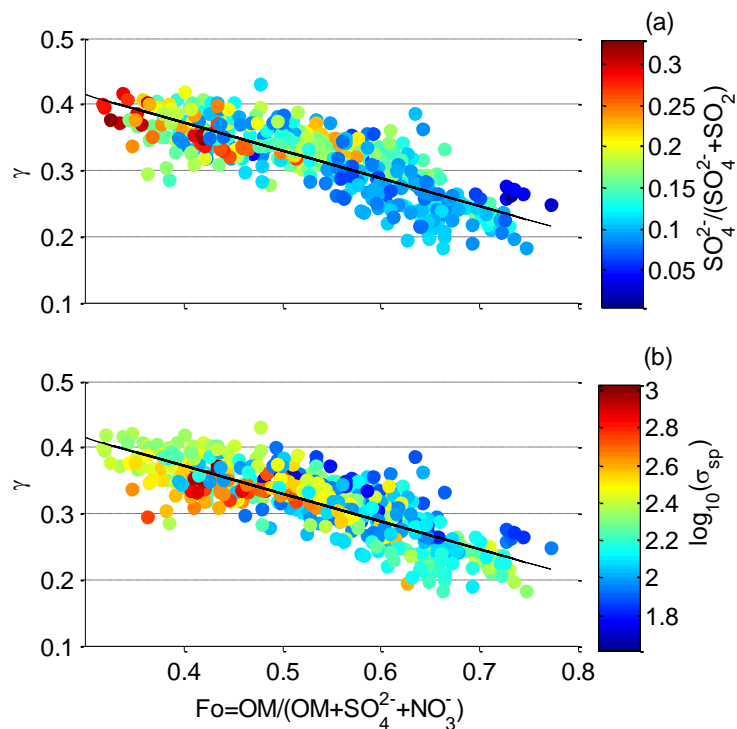
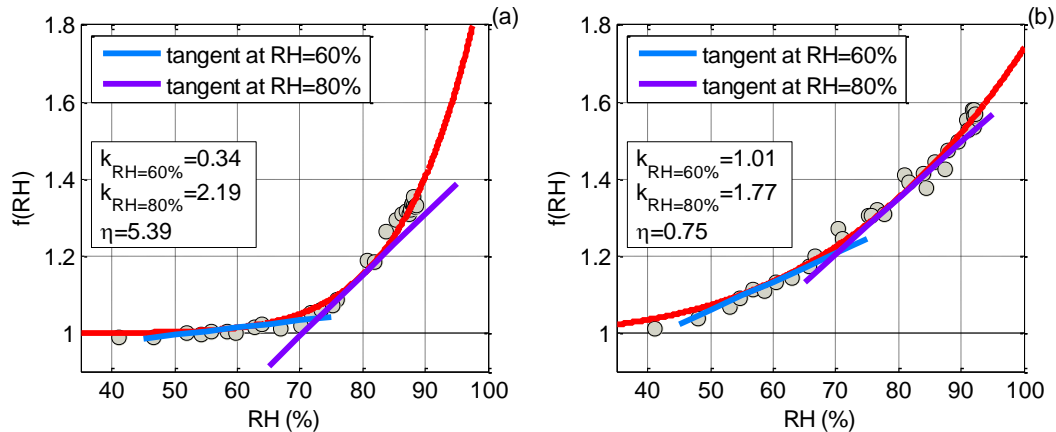
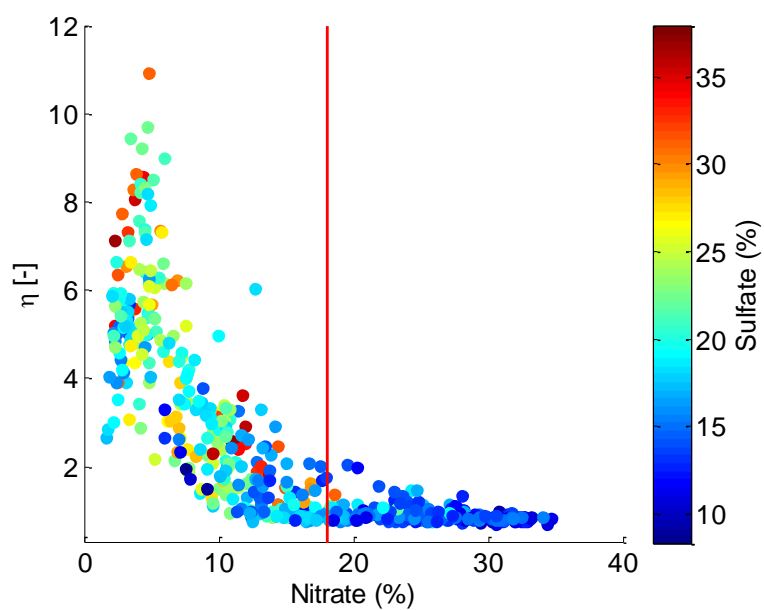


Fig. 10 γ versus $Fo=OM/(OM+SO_4^{2-}+NO_3^-)$ colored by (a) $SO_4^{2-}/(SO_4^{2-}+SO_2)$ molar ratio and (b) $\log_{10}(\sigma_{sp})$.

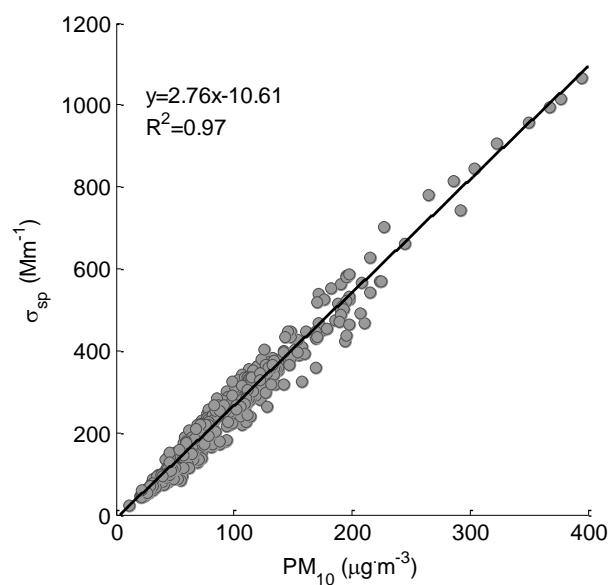


Two distinct examples showing different growth patterns and the corresponding η (a) 2013.03.08 18h $f(RH)$ increased slowly at low RH (usually <70%) and then increase more steeply, thus η is big; (b) 2013.03.10 21h $f(RH)$ increased with at a nearly constant speed-rate and η is small. $k_{RH=60\%}$ and $k_{RH=80\%}$ represent the derivatives at 60% and 80% RH, respectively. $f(RH)$ were-given at 550nm wavelength.



951

952 Fig. 12 Scatter plot of η and the mass percentage of nitrate, colored by the mass
 953 percentage of sulfate.



954

955 Fig. 13 Linear regression of scattering coefficients (σ_{sp}) at 550nm wavelength and
 956 PM_{10} mass concentration.

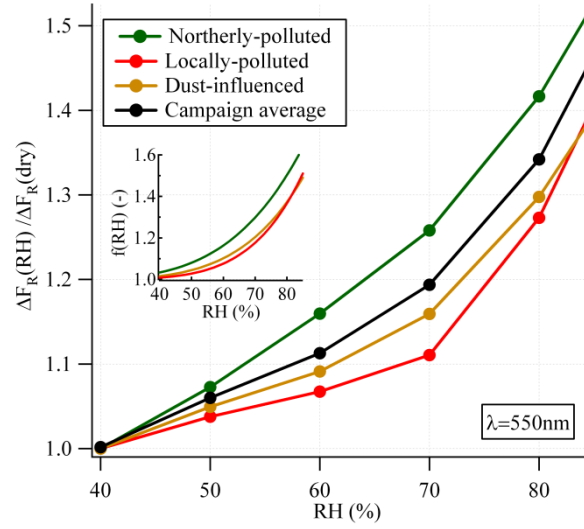


Fig. 14 Influence of relative humidity (RH) on direct radiative forcing for the entire campaign (black line), as well as for the northerly-polluted, locally-polluted and dust-polluted periods, measured by the ratio of radiative forcing at a certain RH to that at dry conditions. The small inlay shows the fitting curves of $f(RH)$ for northerly-polluted, locally-polluted and dust-polluted periods, respectively, using fitting parameters in Table 6. All the parameters were measured at 550nm wavelength.

Table 1 Averaged enhancement factors and mean standard deviations for scattering coefficient, backscattering coefficient and hemispheric backscatter fraction at different RHs (550nm wavelength).

RH(%)	$f(RH)$	$f_b(RH)$	$f_\beta(RH)$
50	1.07(0.04)	1.04(0.02)	0.96(0.02)
60	1.14(0.08)	1.06(0.04)	0.93(0.04)
70	1.24(0.11)	1.10(0.05)	0.89(0.05)
80	1.43(0.12)	1.18(0.07)	0.83(0.05)
85	1.58(0.12)	1.25(0.07)	0.79(0.04)

Table 2 Summary of mass concentrations ($\mu\text{g}\cdot\text{m}^{-3}$) of aerosol species measured by AMS as well as MAAP(*) (SD: standard deviation)

Mean	SD	Minimum	Maximum
------	----	---------	---------

Sulfate	8.1	4.1	0.1	26.1
Nitrate	9.8	12.1	0.2	79.2
Ammonium	6.9	5.5	0.5	42.8
Chloride	1.1	2.0	0.002	22.9
OM	17.7	11.1	2.8	93.9
EBC*	4.1	2.8	0.7	25.3

* EBC was measured by MAAP in PM₁₀.

Table 3 Statistical values of f(85%) at 450 nm, 550 nm and 700 nm wavelengths (SD: standard deviation; prctl: percentile)

λ	mean	SD	90th prctl.	75th prctl.	median	25th prctl.	10th prctl.
450 nm	1.51	0.09	1.63	1.58	1.53	1.47	1.39
550 nm	1.58	0.12	1.72	1.65	1.59	1.49	1.40
700 nm	1.59	0.15	1.77	1.70	1.62	1.46	1.36

Table 4 Average enhancement factors and mean standard deviations for scattering coefficient, backscattering coefficient and hemispheric backscatter fraction in various observation episodes (550nm wavelength).

	Locally-polluted	Northerly-polluted	Dust-influenced
f(80%)	1.36(0.11)	1.50(0.09)	1.37(0.05)
f _b (80%)	1.15(0.06)	1.21(0.06)	1.15(0.03)
f _{β} (80%)	0.85(0.04)	0.81(0.03)	0.84(0.03)
f(85%)	1.52(0.10)	1.64(0.09)	1.48(0.05)
f _b (85%)	1.21(0.06)	1.28(0.06)	1.19(0.04)
f _{β} (85%)	0.80(0.02)	0.78(0.02)	0.81(0.03)
N	295	303	14

Table 5 Curve-fitting parameters of f(RH) at 550nm wavelength for various aerosol types in terms of using equation $f(RH)=c (1-RH)^{-g}$.

c	g	Reference
---	---	-----------

Locally-polluted	0.85±0.08	0.29±0.04	
Northerly-polluted	0.93±0.07	0.28±0.03	This work
Dust-influenced	0.87±0.05	0.27±0.02	
Continental	0.9	0.59	Zieger et al. (2014)
Arctic ^a	1	0.58±0.09	Zieger et al. (2010)
Marine	0.99	0.54	
Polluted	0.59	0.77	Carrico et al. (2003)
Dust	0.60	0.61	
Polluted Marine	1	0.57±0.06	
Dust	1	0.23±0.05	Gass ó et al. (2000)
Clean Marine1 ^b	1	0.69±0.06	
Clean Marine2 ^c	1	0.73±0.07	

982 a fitting results for aerosol samples with RH>75%

983 b fitting results for aerosol samples with RH>60%

984 c fitting results for aerosol samples with RH>80%

985

986 Table 6 Curve-fitting parameters of f(RH) at 550nm wavelength for various aerosol
987 types in terms of Eq. (5).

	a	b	Reference
Locally-polluted	1.24±0.29	5.46±1.90	
Northerly-polluted	1.20±0.21	3.90±1.27	This work
Dust-influenced	1.02±0.19	4.51±0.80	
Clean	1.20±0.06	6.07±0.27	
Polluted	2.30±0.03	6.27±0.10	Pan et al. (2009)
Dust	0.64±0.04	5.17±0.40	
Urban	2.06	3.60	
Mixed	3.26	3.85	Liu et al. (2007)
Marine	4.92	5.04	

988

Table 7 Estimated effects of aerosol hygroscopic growth on direct radiative forcing by locally-polluted, northerly-polluted and dust-influenced aerosols at LinAn, measured by the ratio ($\Delta F_R(RH_{amb})/\Delta F_R(dry)$) of direct aerosol radiative forcing at the ambient average relative humidity ($RH_{amb}=67\%$) for the entire campaign to that in dry condition. All the parameters were measured at 550nm wavelength.

	$f(RH_{amb})$	$b(dry)$	$\bar{\beta}(dry)$	$b(RH_{amb})$	$\bar{\beta}(RH_{amb})$	$\Delta F_R(RH_{amb})/\Delta F_R(dry)$
Entire campaign	1.21	0.126	0.268	0.115	0.255	1.157
Locally-polluted	1.17	0.131	0.274	0.123	0.263	1.118
Northerly-polluted	1.26	0.121	0.262	0.106	0.243	1.195
Dust-influenced	1.15	0.146	0.289	0.132	0.274	1.105